Master Thesis

Deggendorf Institute of Technology

Faculty of Applied Natural Sciences and Industrial Engineering

Master Mechatronic and Cyber-Physical Systems

Time- domain based passivity approach für Kopplungssteuerung mit variabler Steifigkeit in bilateraler Teleoperation

Time- domain based passivity approach for coupling control with variable stiffness in bilateral teleoperation

Master thesis to obtain the academic degree:

Master of Engineering (M.Eng.)

submitted by: Revanth Bhadravathi Prakash,
Munich, 00776839

first examiner: Prof. Dr.-Ing. Wolfgang Aumer

supervisor : Dr. Michael Panzirsch

Munich, 30.04.2021

Declaration

Name of the student: Bhadravathi Prakash Revanth

Name of the first examiner: Prof.Dr-Ing Wolfgang Aumer

title of the master thesis:

Time- domain based passivity approach for coupling control with variable stiffness in bilateral teleoperation

1. I hereby declare that I have written this master thesis independently. I have not submitted it for any other examination purposes. I have not used other references or material than mentioned in the bibliography and I have marked all literal and analogous citations.

Cham, (date) 30.04.2021 signature of student: Digitally signed by Revanth Bhadravathi Prakash DN: cn=Revanth Bhadravathi Prakash, o=Revanth, ou=Revanth, email=revanprak252@gmail.com, c=US Date: 2020.11.05 02:24:42 +01'00'

2. I agree that my master thesis may be made available to a broader public by the DIT library. Therefore, I hand in a further bound copy of my master thesis.

☒ yes ☐ no

Cham, (date) 30.04.2021 signature of student: Digitally signed by Revanth Bhadravathi Prakash DN: cn=Revanth Bhadravathi Prakash, o=Revanth, ou=Revanth, email=revanprak252@gmail.com, c=US Date: 2020.11.05 02:25:10 +01'00'

I declare and take the responsibility that I am the exclusive owner of all rights concerning the master thesis, including the right of disposal concerning drafts and attached illustrations, plans or similar and that no third party rights or claims or legal requirements will be made upon making this master thesis publicly available.

To be filled in by the first examiner in the event that the author agrees with public accessibility of the master thesis:

Adding a copy of the master thesis into the stock of the library and lending the copy is:

☐ approved ☐ not approved

Cham, (date) ___________ signature of first examiner: ___________________________

Acknowledgment

First of all, I would like to express my sincere gratitude to Dr.Michael Panzirsch and Prof. Dr.-Ing. Wolfgang Aumer for their outstanding support and valuable guidelines throughout my Master thesis. Without their encouragement, constructive criticism, and constant feedback, my thesis work would not have been achievable. I would also like to thank Mr. Marek Sierotowicz and Dr. Harsimran Singh, whose advice and insights were invaluable to me. Robotics is an exceptional research domain that demands collaborative interactions and keen enthusiasm. Thus, it is extremely important to work within a team of innovative and enthusiastic people. I am also thankful for the Analysis and Control of the complex robot systems department at the German Aerospace Center (DLR) which provided me an international and dynamic working environment, with the possibility of meeting and working with many outstanding researchers.

I am also thankful to my mother, Vrundha Kala, for her love and support throughout the years. I am grateful to my father, Dr.B.G Prakash, who always gave me wise and insightful counsel. I would like to thank my brother, Dr.Yashwanth Prakash, for being supportive throughout my studies.

Abstract

In the field of bilateral teleoperation, achieving transparency, which refers to the quality of immersion of the operator in the remote environment and ensuring passivity has been major parameters for obtaining a stable controller design. Especially after the contact with the environment, when the variable impedance is introduced, kinetic energy is generated into the system. In one of the most critical cases of a narrow passage, and especially in combination with delay, this can lead to a divergent bouncing between two close walls and leads to jeopardizing the system's stability. Therefore the passivity control becomes crucial in these scenarios. The Time-domain Passivity Approach (TDPA) and the state-of-the-art approach of TDPA, which considers the energy reflection (TDPA-ER) assures stability in the presence of delay and has already been validated in many teleoperation scenarios. To solve the problem of energy generation caused by variable impedance, a new methodology that assures passivity was required. The main contributions of thesis work include analyzing and testing of TDPA-ER for the first time with variable impedance and a new impedance control strategy that uses the concept of stiffness gradient was developed to accommodate for the time-varying stiffness. This proposed method is augmented with the conventional TDPA and TDPA-ER. To demonstrate the validity of the proposed approach, several simulations considering different case scenarios are conducted. Then, to prove the effectiveness of the proposed strategy, experiments were performed with the 1-DOF rotational devices with the varying stiffness estimated from a Myo-Band attached to a user's arm. And finally, a possible extension of the proposed approach has been presented.

Contents

Chapter 1

Introduction

A Teleoperation (*tele* derived from Greek meaning: distant) system provides an extension for human capabilities to perform various tasks at very far distant places. These systems are mainly adopted in order to keep humans safe from a hazardous environment, reduce the cost of travel, and facilitate many other complex tasks which are not easily achieved by human beings. It encompasses the various types of applications including space operation and underwater exploration via teleoperation [1] [2], Minimal invasive surgeries [3] [4] [5] represents another important application in the field of teleoperation. The concept of teleoperation is also applied to teach new skills to humans [6] [7] [8] [9]. The teleoperation setup is as shown in the figure 1.1. The human operator operates the main device located at the local site and

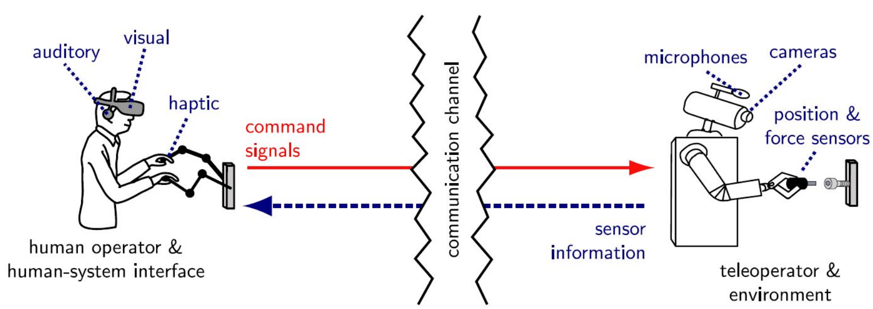

Figure 1.1: Model of a teleoperation system

controls the secondary device at the remote site. The communication channel provides a communication between the two devices devices which are at different location. The sensory information from the human operator is sent via communication channel (CC) to the secondary device side in order to perform desired actions. The force feedback provides useful source for the manipulation tasks and thereby ensuring smooth operation and increased performance [10] [11]. The haptic devices are comprised of tactile sensors that measure the position exerted by the user on the interface and it also perceives information from the secondary device about the remote environment in the form of tactile and force feedback. The force feedback produces directional forces, which is calculated from a coupling stiffness.

1.1 Motivation

In the domain of teleoperation, despite the continuous improvements and advancements in the field of control and stability of teleoperation system, there are still many tasks and operations, that cannot be conducted under sensory feedback signals. For example, tasks that are usually performed by humans with ease such as drilling, chipping, or catching a ball in hand and many other activities involving large uncertainty in the environmental constraints cannot be easily performed by conventional bilateral teleoperation due to inadequate or low quality sensory information (such as position, force, velocity).

During the teleoperation, when the secondary device is approaching an object and when the delay is high, and if in case the impedance controller is set for high stiffness, the impact would lead to damage both the secondary device robot and the object or environment. Furthermore, if high unexpected forces are generated and is fed back to the user with delay, this causes injury to the operator.

The humans on the other hand have a stable mechanism to be compliant with the unknown environment. Inspired by the superior functional capabilities and interaction performance of human limbs the concept of variable impedance control can be used as an alternative to the position based control or bilateral force control methods. Variable impedance is a control criterion wherein through the method of teleoperation a secondary device (output device) is controlled through an impedance controller by measuring and replicating the user's limb pose or the muscle impedance profile in real-time. The impedance of the user is estimated by monitoring the muscle activity through surface Electromyography (sEMG). This combined reference command i.e position and impedance is sent to the coupling controller of the teleoperated robot in-order to accomplish a particular task [12]. Incorporating the human motor control principles into the controllers of robots will enhance the performance and allow the interaction capabilities close to those achieved by the humans even in the case of changes or uncertainties in the dynamic environment.

Many methodologies have been developed that deal with the variable impedance, the most common method being the tank-based approach. Even though this approach shows satisfactory results in simulations and experiments, the consideration of already dissipated energy is often criticized. In this work, we focus on a concept that gives satisfactory results, which is purely based on potential energies and is physically more comprehensive.

It can be seen in [13], the authors propose the concept of observer-based force gradient controller in which the undesired increase in force generated by the delay in the communication channel is reduced and results in minimizing the high-frequency vibrations caused by the TDPA. Inspired by this approach the principle of the gradient is used and a new method called stiffness gradient control is presented in this work which adopts the variable stiffness commanded from the sensor and ensures passivity in the teleoperation system.

1.2 Organization of the report

The following chapters of this work are structured as follows:

Chapter 2 includes a brief background about the methods in bilateral teleoperation, fundamentals of Time Domain Passivity Approach and state-of-the-art approaches in TDPA of delayed 2-ports and limitations resulting from the direction-dependent energy monitoring is presented. The concept of variable impedance was introduced. Furthermore, related work to this thesis are discussed.

Chapter 3 describes the problem statement in more detail. The passivity problems due to variable stiffness and the discussion of state-of-the-art approach are mainly presented.

Chapter 4 describes the proposed control approaches to solve the problem and the concept of stiffness gradient approach is introduced along with its implementation in passive time-delayed teleoperation with adaptive impedance is presented.

Chapter 5 In this chapter, the simulation results are presented based on the implementation of the stiffness gradient concept to the passive time-delayed teleoperation with adaptive impedance and relative experimental validation is performed.

Chapter 6 This chapter summarizes the work presented in this thesis and the possible future work on this topic is also discussed.

Chapter 2

Background

2.1 Bilateral teleoperation

This chapter mainly focuses on the methods, which are used to design a bilateral teleoperation system, and are based on two different system representations. For the design of the control architecture and the design of the controller parameters, the model-based signal flow representation is used, which considers an idealized system. Then, the energy-based model-independent network representation of the system is used to take into account the influence of time delays.

The signal flow architecture of bilateral teleoperation system is as shown in figure 2.1. It consists of a human operator (HO), main device (input device), secondary device (output device), the environment (EN), the controller system (PD controller), and the communication channel (CC), which is represented by the time delays T_1 and T_2. The time delay T_1 acts in the direction of the main device to the secondary device and T_2 in the opposite direction.

In the signal flow diagram of a bilateral teleoperation system, velocities are usually entered instead of positions, since this velocity and the force signals are always conjugate pairs, and the product of this results in power.

All components in the system except for the communication channel exhibit either impedance or an admittance characteristic. An admittance type represents a dynamic mapping from forces to positions or velocities, while an impedance performs the inverse mapping from positions or velocities to forces. If the impedance and admittance mappings are assumed to be linear

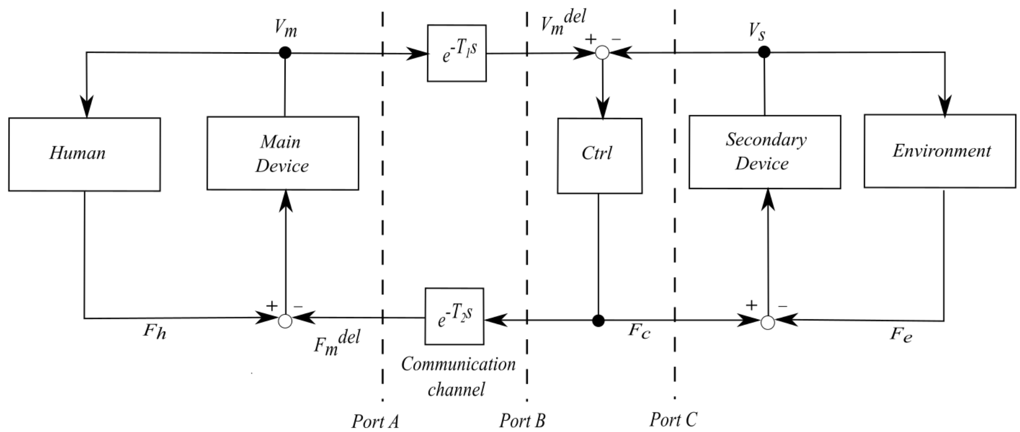

Figure 2.1: Signal flow of PF control architecture in bilateral teleoperation system: The communication channel is represented by two-time delays. T_1 and T_2. The velocity v_m as well as v_s correspond to the velocity of main and secondary device respectively. The velocity v_m is transmitted to the coupling controller on the secondary device side delayed by the time delay T_1. This controller determines from the difference of the delayed main device velocity v_m^{del} and the secondary device velocity v_s, this controller determines the force F_c, which is necessary to adapt the positions of the secondary and the main device. The force signal F_c arrives delayed by T_2 delayed at the main device side.

and time-invariant (LTI), corresponding transfer functions can be derived using the Laplace transformation. And impedance mappings Z(s) are defined as:

$$Z = F(s)/v(s).$$

The widely accepted human and environment systems behavior can be modeled as mass-damper-spring system as:

$$Z_h(s) = \frac{M_h s^2 + B_h s + K_h}{s}.,$$

$$Z_e(s) = \frac{M_e s^2 + B_e s + K_e}{s}.$$

where M_h, B_h, K_h, B_e, K_e are the mass, damper and spring components of the human and the environment and Z_h, Z_e are the human and environment impedances. Similarly the simplified model of the main device and secondary device can be described by the mass-damper system or even a single mass.

$$Z_M(s) = M_M s + B_M.$$

$$Z_S(s) = M_S s + B_S.$$

M_M, B_M, M_S, B_S are mass and damping components of main and secondary devices respectively, and $Z_M$and Z_S are their impedance.
Admittance mapping Y(s) is represented as:

$$Y = Z^{-1} = \frac{v(s)}{F(s)}.$$

$$Y_M(s) = \frac{s}{M_M s^2 + B_S s}.$$

$$Y_S(s) = \frac{s}{M_S s^2 + B_S s}.$$

M_M, B_M, M_S, B_S are mass and damping components of main and secondary devices respectively, and $Y_M$and Y_S are their admittance.
For the PD controller (PI equivalent if the input is velocity), which is widely used in the field of teleoperation. The equivalent impedance is given by:

$$Z_c(s) = \frac{Bs+K}{s}$$

where 'B' and 'K' are virtual damping and the stiffness values, which is, derivative and proportional gains respectively.
The role of the impedance controller is to reduce the position error or deviation between the main device and the secondary device. The controller compares the velocities of the two devices and generates the force (F_c) which is sent to the main and secondary device to align their position.

2.1.1 Control Architecture

The names of the control architectures denote the signals transmitted over the communication channel. The first part of the name refers to the signal transmitted from the main device to the secondary device and the second to the signal flowing in the opposite direction. In the following different PF (Position-Force) architectures are discussed. These were developed for different application scenarios in the field of robotics.

Position-Force computed architecture

The (P-Fc) control architecture is represented as shown in the figure 2.1 a PI controller is provided on the secondary device side. In this way the main device receives the controller force with a delay, this limits the stability and position sequence of the system. The advantage of this architecture is that, conjugate signals flow through the communication channel. This simplifies for the implementation of the Time Domain Passivity Approach, as will be explained in the further sections.

P-F measured architecture

The P-F measured architecture is as shown in the figure 2.2. In this control architecture, the main device receives force feedback, that is perceived by the force or torque sensor on the robot, which comes in contact with the environment. But the secondary device receives the computed force from the PI controller. This approach is more robust and intuitive in terms of sensing the environment compared to the previous (P-Fc) architecture. More details of this approach are given in [14]. In-terms of stability and performance the feedback force can be controlled by scaling.

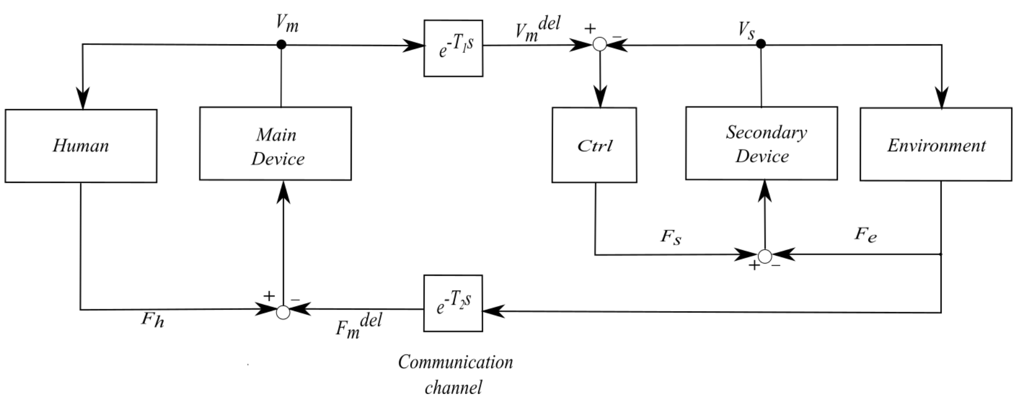

Figure 2.2: Block diagram of PF-Measured control architecture

2.1.2 Network Representation

The network representation of a bilateral teleoperation system is as shown in figure 2.4. The usage of network representation provides as an important tools for representing a teleoperation system as it mainly allows to obtain conclusions regarding the passivity of the system by examining the input and output energy flows of each subsystem. At each port, a power conjugate pair of effort variable (force) and flow variable (velocity) can be defined and measured. By integrating this power conjugate pair over time, the total energy can be calculated. Also, considering the sign of the conjugate pair, the energy flow direction can be determined.
One of the other advantages of using this representation is a generalized system analysis, which means, the passivity condition can be applied on every system as long as it is represented as network elements.
This type of representation of a bilateral teleoperation systems can be represented by the 1-port subsystems as shown in figure 2.3a

a) 1-portsubsystem

b) 2-portsubsystem

Figure 2.3: Network subsystem representation

(also "1-port", or "two-pole") which includes operator and environment and the 2-port subsystems (also "2-port", or "quadripole") is indicated as shown in figure 2.3b. This includes Main device, PI controller, communication channel and Secondary device. Multiple 2-port subsystems, such as the PI/PD controller and the communication channel, can be combined into a single 2-port subsystem. This would then be ended by the two 1-port subsystems combined which contain main device and human operator, or secondary device and environment as shown in figure 2.5.

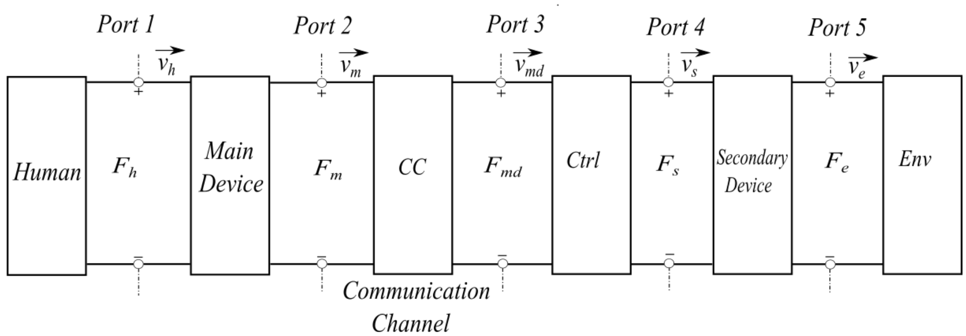

Figure 2.4: Network representation of Bilateral Teleoperation

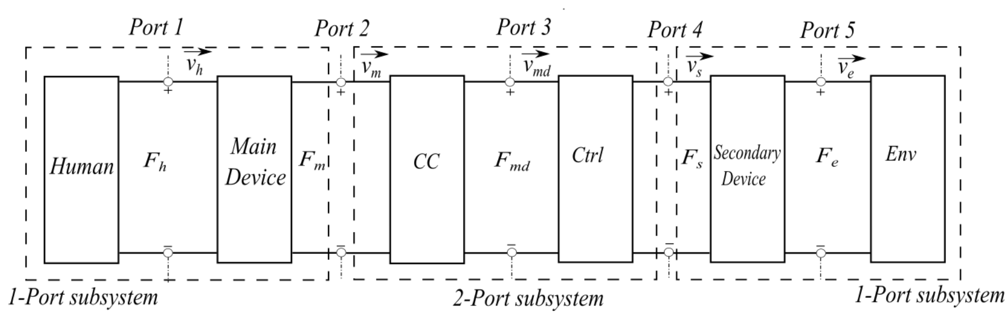

Figure 2.5: Network representation of subsystems in Bilateral Teleoperation

2.2 Time Domain Passivity Approach in Bilateral Teleoperation

The stability in bilateral teleoperation is usually achieved if the system is passive (e.g. controlled via passivity control) or in the case of low delays in

the communication channel. However, if the system is designed to be always passive then no constant dissipation or damping is required. This results can lead the system to be too conservative and might in-turn reduce the transparency [15]. In order to overcome this issue, a new stability ensuring approach called Time Domain Passivity approach (from here on: TDPA) has been designed. The TDPA has been presented in [16] and then this approach was extended to position-position [17] and 4-channel architecture [18] [19]. The TDPA is an approach that monitors the energy of the system in real-time and uses adaptive dissipative control method only when the system shows an active behavior to maintain the passivity of the system. As the name suggests the dissipation is computed in the time domain as a function of energy observed of the network.
The TDPA has become one of the most commonly used methods in the field of teleoperation, since it does not assume anything but accepts any form of energy generation without requiring the model of energy source. The TDPA has already been successfully applied in the field of teleoperation [20] [21] [17] in the field of haptics [22] [23] and mechanical multibody systems [24].
In the ideal case of the teleoperation system, which is the combination of both one and two-port subsystems, it assumes to be a transparent network, where input and output signals are identical and is usually characterized by communication with zero transmission delay. But whereas during the real case scenario, the transmission delay is present in the communication channel, that leads to active behavior and thus makes the system unstable.
In order to overcome this issue, an impedance and admittance type passivity controllers are added on each side of the communication channel as shown in the figure 2.6

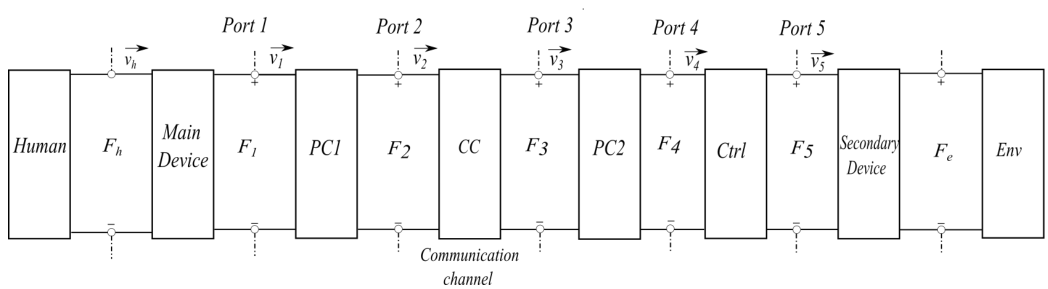

Figure 2.6: Network representation of Bilateral Teleoperation with Passivity controllers

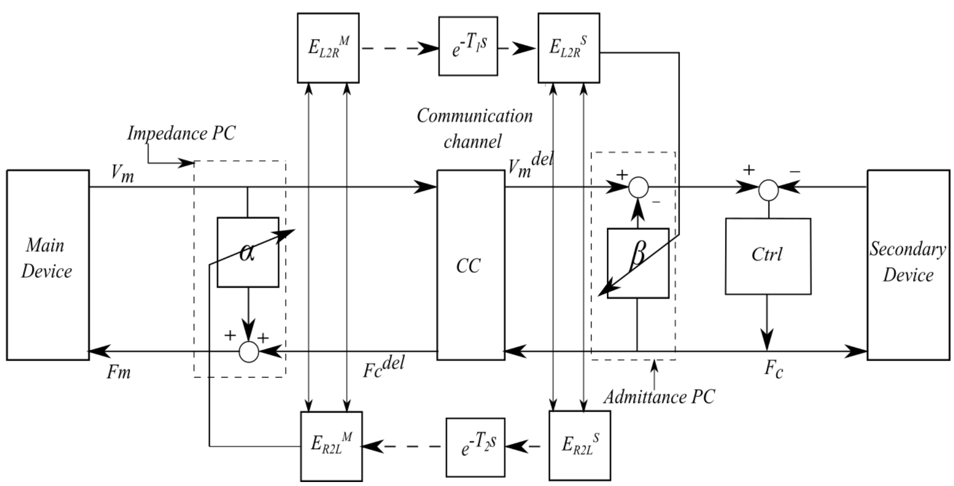

Figure 2.7: Signal flow diagram of TDPA

The signal flow diagram as shown in figure 2.7 has two passivity observers (POs) and are attached to each port of the network in order to monitor the input energies and output energies. The passivity controllers (PCs) are placed

on either side of the communication channel. The PC at the left side of the channel is the impedance type PC and at the right side, the admittance type PC is present. The input energy at the main device side (E^M_{L2R}) is monitored and is sent to the secondary device side. The damping element 'β' is varied such that it reduces the output energy of the secondary device E^S_{L2R} below the delayed input energy in order to satisfy the passivity condition. The same procedure applies for the energy flow in the opposite direction from the secondary device to the main device.
From the network representation of bilateral teleoperation as shown in figure 2.6 it can be seen that velocity and force are exchanged between the main device and secondary device. To maintain the stability of the system, the passivity criterion for the communication channel (two-port network) has to be considered. The equation for the passivity observer is given by [25]:

$$E_{obs} = \Delta T \sum_{k=0}^{n} [f_m(k) v_m(k) - f_s(k) v_{md}(k)]. \tag{2.1}$$

Where 'ΔT' stands for sampling time, f_m, v_m are force and velocity of main device and f_s, v_{md} are force of the secondary device and delayed main device velocity respectively. Considering the above equation, it is clear that it is not possible to monitor the energies at each side of the two-port simultaneously because of the inevitable delay induced in the communication channel. To overcome this problem a solution is proposed in [25]. Here this can be improved by monitor the energy at each side of the channel and transmit it over the communication channel (CC). As shown in figure 2.8 the energies are further parted into directions in which the energy flows, such as 'L2R' represents left to right directions and 'R2L' denotes right to left direction at the main device and secondary device sides and can be computed as:

$$E^M_{L2R}(t) = \begin{cases} E^M_{L2R}(t-1) + \Delta \mathrm{T} \cdot P_m(t), & \text{if } P_m(t) > 0. \\ E^M_{L2R}(t-1), & \text{if } P_m(t) \leq 0. \end{cases} \tag{2.2}$$

$$E^S_{R2L}(t) = \begin{cases} E^S_{R2L}(t-1) + \Delta \mathrm{T} \cdot P_s(t), & \text{if } P_s(t) > 0. \\ E^S_{R2L}(t-1), & \text{if } P_s(t) \leq 0. \end{cases} \tag{2.3}$$

$$E^M_{R2L}(t) = \begin{cases} E^M_{R2L}(t-1), & \text{if } P_m(t) > 0 \\ E^M_{R2L}(t-1) - \Delta\mathrm{T}{\cdot}P_m(t), & \text{if } P_m(t) \leq 0. \end{cases} \tag{2.4}$$

$$E^S_{L2R}(t) = \begin{cases} E^S_{L2R}(t-1), & \text{if } P_s(t) > 0 \\ E^S_{L2R}(t-1) - \Delta\mathrm{T}{\cdot}P_s(t), & \text{if } P_s(t) \leq 0. \end{cases} \tag{2.5}$$

where the power generated at an instant 't' at port i and is given by:

$$P_i(t) = f_i(t)v_i(t). \tag{2.6}$$

The Passivity Observers are located at each side of the communication channel and the energy observed can be calculated as:

$$W^{PC2}(t) = E^M_{L2R}(t - T_1) - E^S_{L2R}(t) - W^{PC2}_{diss}(t-1). \tag{2.7}$$

$$W^{PC1}(t) = E^S_{R2L}(t - T_2) - E^M_{R2L}(t) - W^{PC1}_{diss}(t-1). \tag{2.8}$$

Where $W^{PC1}(t)$ represents the observed energy that has to be dissipated by the passivity controller (from here on:PC) in the R2L direction and $W^{PC2}(t)$ represents the observed energy that has to dissipated by the PC in the L2R direction at the time step 't'. T_1 and T_2 denotes time delay in L2R and R2L directions respectively.

The stability of the system is ensured if the following passivity criteria for the TDPA is met:

$$E^M_{L2R}(t) - E^M_{R2L}(t) + E^S_{L2R}(t) - E^S_{R2L}(t). \geq 0, \forall t \geq 0 \tag{2.9}$$

The passivity controllers are designed to act as a variable damper to dissipate active energy observed by the passivity observers.
With the given passivity conditions the, impedance type PC on the main device side can be computed as:

$$\alpha(t) = \begin{cases} \frac{-W^{PC1}(t)}{\Delta T \cdot \dot{x_m}^2(t)}, & \text{if } W^{PC1}(t) < 0. \\ 0, & \text{if } W^{PC1}(t) \geq 0. \end{cases} \tag{2.10}$$

$$f_m(t) = f_{md}(t) + \alpha(t)v_m(t). \tag{2.11}$$

As a result the feedback force to the main device (f_{md}) is modified by the virtue of the adaptive coefficient'α'.
and for the admittance type passivity controller on the secondary device side can be calculated as:

$$\beta(t) = \begin{cases} \frac{-W_{PC2}(t)}{\Delta T \cdot f_s^2(n)}, & \text{if } W_{PC2}(t) < 0. \\ 0, & \text{if } W_{PC2}(t) \geq 0. \end{cases} \tag{2.12}$$

$$v_s(t) = v_{sd}(t) + \beta(t) f_s(t). \tag{2.13}$$

As a result, the desired velocity of the secondary robot (v_{sd}) is modified by the virtue of the adaptive coefficient 'β'.
This designed TDPA shows jittering effects, when the feedback force is sent to the Human operator in the experiments. To overcome the force jittering effects, [25] has proposed using a passive virtual system composed of mass (mc) and spring (kc) which is placed in-between the main device and impedance PC as shown in figure 2.9, which acts as a bidirectional low pass filter that removes the high frequency force signals while still maintaining system passivity.

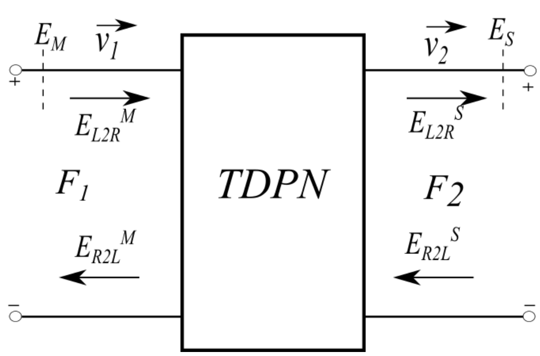

Figure 2.8: TDPN Energy flow[26]

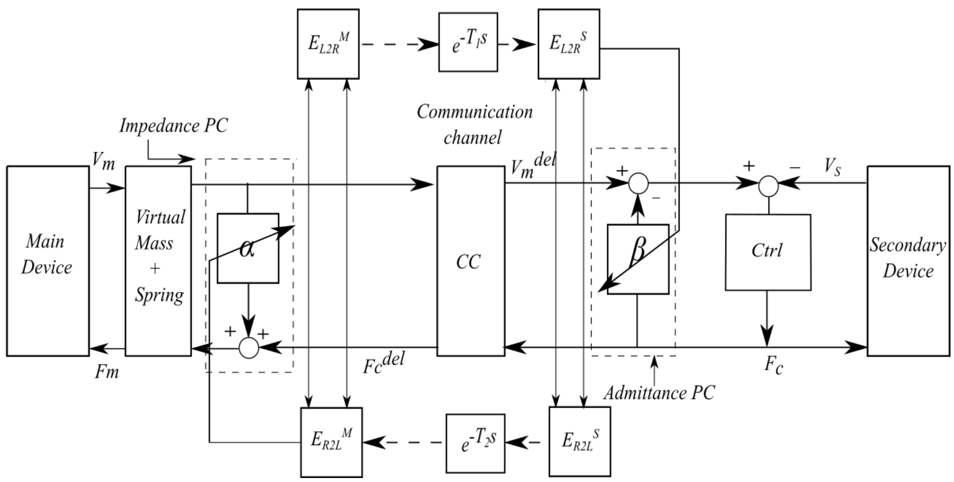

Figure 2.9: A time-delayed teleoperation system with the proposed two-port TDPA and the virtual mass with spring.

Drawbacks of TDPA

The TDPA approach, however convenient it might seem it has drawbacks of its own. The energy storage element is excluded from the passivity analysis based on the assumption that it does not hamper the conditions for passivity. The admittance type PC is used on the secondary device side, leads to position drift and thus leads to instability.

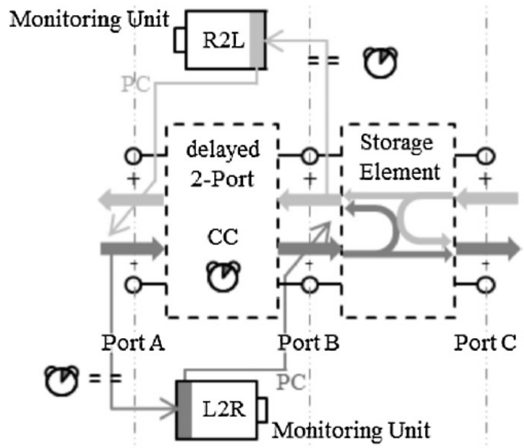

Figure 2.10: Energy observation and Passivity control in conventional TDPA [27].

In this traditional approach, the passivity controller as shown in figure 2.10 is located at port B before the energy storage element. The PC dissipates energy coming from the main device side (L2R direction) and this leads to charging up of the storage element less than intended that can change the coupling behavior drastically and thus leading to over-conservative dissipation of energy (R2L direction) and results in position drift. Several methods are proposed to compensate for this position drift [27] [28] [29]. But however, as per the experiments conducted in [30], during the case of high time delay the compensation is limited.

After consideration of all these drawbacks of the conventional TDPA, a less conservative approach is proposed in [30] and will be explained in detail in the upcoming sections 2.3 .

2.3 Energy reflection based Time Domain Passivity Approach

In this approach, the energy reflection of the energy storage element is considered for the passivity analysis. figure 2.11 presents a basic idea of the proposed control architecture. The two PCs are located at port A and port

C to include the energy storage element together with the communication channel (CC) in the passivity-controlled delayed two-port network. This architecture is similar to the approach presented in [31] [32] .But however, in contrast to the conventional architectures, where these approaches consider uni-directional observation and control, in this method an energy monitoring unit (battery shaped) collects an available amount of energy and distributes in both directions of the delayed two port network. Since the energy monitoring unit has a physical relationship with the energy storage element it is located at the right side of the communication channel as shown in figure 2.11.

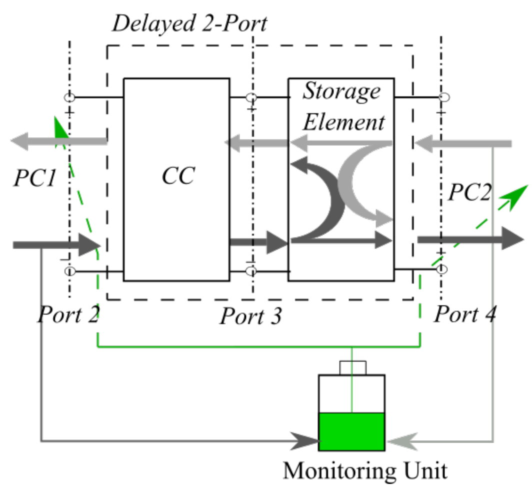

Figure 2.11: Proposed energy observation and passivity control approach considering energy reflection [30]

The energy monitoring unit is charged up by the dark gray arrow (Port 2) and light gray arrow (Port 4) which indicates the power input from both the L2R and R2L direction respectively. The dashed arrow represents the position of passivity controllers (PC), which dissipates an excess amount of energy, taking into consideration the amount of available energy in the monitoring unit.

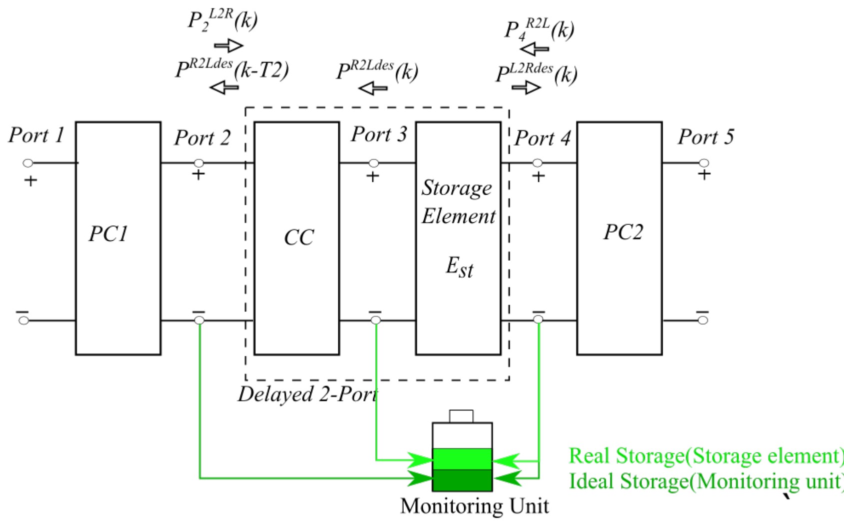

Figure 2.12: Real and Ideal potential energy storages[30]

The figure 2.12 represents the difference between real and ideal energy storage in the monitoring unit. The real storage is filled by port 3 and port 4 from L2R and R2L directions respectively and the ideal storage is filled up by the power entering from port 2 (P_2^{L2R}) and port 4 (P_4^{R2L}). This ideal storage build-up is regarded as the desired energy content of the controller as this energy is introduced into the 2-port system by the main and secondary device. This built-up energy in the ideal storage (energy monitoring unit) leaves port 2 in the R2L direction and port 4 in the L2R direction. But the desired power output $P^{L2R,des}$, $P^{R2L,des}$ leaving at both the ports in two directions is calculated with the control logic as presented below.
The ideal energy storage $E_{st}(k)$ in the monitoring unit which is built up by the Main (Input device) or Secondary device (output device)is given by:

$$E_{st}(K) = E_{st}(k-1) + P_2^{L2R}(k-T_1)T_s + P_4^{R2L}(k)T_s. \tag{2.14}$$

As we can observe from the above equation the power $P_3^{L2R}(k)$ measured at port 3 is not used for building up the storage because this energy is affected

by the delay in the communication channel(CC). And therefore the delayed input energy from port 2 has to be used as input instead.
The calculation of passivity control logic is split into two parts, wherein at first, the excessive amount of energy that leaves the energy storage element is computed. This energy might lead to instability in the system because of energy injection into the storage element by the communication channel in the L2R direction. The actual power output in both the directions is given by:

$$P_{out}^{act}(k) = P_3^{R2L}(k) + P_4^{L2R}(k). \tag{2.15}$$

And now for the second part, the desired or allowed output power is to be calculated to ensure passivity. For this purpose, the proposed logic is designed in such a way that, if the output power at port 3 and port 4 ($P_{out}^{act}(k) = P_3^{R2L}(k) + P_4^{L2R}(k)$) is less than the stored energy in the energy storage element, then the same amount of energy is assigned at their respective port. Otherwise, all the energies in the energy storage element are assigned to the main device and the secondary device by the ratios of P_3^{R2L} and P_4^{L2R} in $P_{out}(k)$.

$$P^{R2L,des}(k) = \begin{cases} \frac{E_{st}(k)}{T_s}\frac{P_3^{R2L}}{P_{out}(k)}, & \text{if } E_{st}(k) < P_{out}(k)T_s. \\ P_3^{R2L}(k), & \text{if } E_{st}(k) \geq P_{out}(k)T_s. \end{cases} \tag{2.16}$$

$$P^{L2R,des}(k) = \begin{cases} \frac{E_{st}(k)}{T_s}\frac{P_4^{L2R}}{P_{out}(k)}, & \text{if } E_{st}(k) < P_{out}(k)T_s. \\ P_4^{L2R}(k), & \text{if } E_{st}(k) \geq P_{out}(k)T_s. \end{cases} \tag{2.17}$$

This desired power $P^{L2R,des}(k)$ and $P^{R2L,des}(k)$ is sent to the main device and secondary device side that are integrated over time for passivity control. The passivity controller on the main device side has to make sure that not more energy than $E^{R2L,des}(k) = \sum_{j=0}^{k-T_2} P^{R2L,des}(j)T_s$ leaves the port. Excess of energy dissipated is given by:

$$W^{PC1}(k) = E^{R2L,des}(k) - E_2^{R2L}(k) - W_{diss}^{PC1}(k-1). \tag{2.18}$$

where $E_2^{R2L} = \sum_{j=0}^{k} P_2^{R2L}(j)T_s$ is the uncontrolled energy output at the port 2 and $W_{diss}^{PC1}(k-1)$ is the sum of energy dissipated at previous time step.
Similarly, the passivity controller at the secondary device side is given by:

$$W^{PC2}(k) = E^{L2R,des}(k) - E_4^{L2R}(k) - W_{diss}^{PC2}(k-1). \tag{2.19}$$

Since on both sides the impedance type passivity controllers are used, this results in force generation with high frequencies due to the sudden force changes. Therefore to compensate for this effect, The author in [25] propose a passive virtual mass-spring system that acts as a low pass filter of force and velocity in both directions and helps in minimizing this effect.
In the next step, The energy storage in the energy monitoring unit has to be updated by subtracting the powers P_3^{R2L} and P_4^{L2R} since they have exited the ports in the respective direction.

$$\begin{aligned} E_{st}(k) = E_{st}(k-1) + (&P_2^{L2R}(k-T_1) + P_4^{R2L}(k) \\ &- P_3^{R2L}(k) - P_4^{L2R}(k))T_s. \end{aligned} \tag{2.20}$$

2.4 EMG-based impedance estimation

In order to estimate the stiffness of the user's arm at the wrist level, the MYO armband is used. This sensor has 8 EMG channels. The articles [33] [34] [35] describe the machine learning algorithms that are used for the estimation of intended stiffness, but are normally used to estimate the user's hand movement intention in terms of a desired hand pose. The most recent one describes the algorithm in more general terms, whereas the other two describe the algorithm in more detail. In this, the concept of supervised incremental learning approach is proposed in order to estimate the grasping pattern and to predict the finger forces from the sEMG. The algorithm adopted is Ridge Regression (RR) in order to estimate finger forces using ultrasound imaging [36] however, since the proposed linear models would not be sufficient to model the relationship between the sEMG and finger forces the author combined incremental RR with Random Fourier features (RFF's) to generalize over non-linearities. This is referred to as incremental ridge regression with Random Fourier features (iRFFRR).

2.5 Related work

Considerable efforts have been made in recent years for developing appropriate impedance control strategies for smooth human-robot physical interaction by learning and adopting impedance variation strategies from human beings.
The tank-based approach is one such method in which they [37] provide a new impedance control strategy to accommodate for variable stiffness by properly controlling the energy exchanged between the subsystems during the action. With this control approach, the passivity of the system is guaranteed for any given choice of the stiffness variation and the system provides stability in both free motions and the case of impact with the environment. The variation of stiffness produces extra energy which is injected into the system and thus leading to phases of energy generation and potentially to instability. This loss of the passivity affects impedance control and hence due to this, the stable interaction is not guaranteed. For example, in one of the most critical cases of a narrow passage, and especially in combination with delay, this can lead to a divergent bouncing between two close walls. In order to avoid such issues, the traditional impedance control model is combined with tank storage (which stores the dissipated energy from the system), which is energetically coupled through the input, this allows the stiffness variation by still maintaining the passivity and stable interaction behavior with the environment. The tank-based approach was first introduced in the [38] and later on, it was adopted by [39] [40] in the field of teleoperation of robots.
In the case of the tanks approach the dissipation element of the system is replaced by the storing element (tanks). This tank is usually used for storing dissipated energy and this stored energy is released to the system, which is used for other control purposes (e.g.variable stiffness) behavior on the secondary device side or compensation for the position error between the main and secondary device side). Both these elements(tanks and dissipative elements) process the energy in a very different manner. The tanks always perform a reversible transfer of energy (i.e. the energy can be absorbed and released) into the system. But whereas the energy dissipative elements perform an irreversible transfer of energy (energy can only be absorbed). Considering all these advantages of tanks the authors implement them in the context of impedance control. To limit the absorption or exchange of energy between the system and tank, a design parameter is formulated which enables/disables the storage of energy.

The tank is augmented with the impedance model and is energetically coupled through an input. The control logic of the input is designed in such a way that it decides whether to incorporate variable stiffness or not. If the energy of the tank is greater than the certain threshold then this provides an opportunity for the system to accommodate the desired variable stiffness behavior and on the contrary, if the energy content of the tank is lower than a certain defined threshold then the system has to implement constant stiffness behavior.
Simulations and experiments are performed to test the effectiveness of this approach. In the case of simulation, the main goal of the authors was to test the stability of the system while implementing a periodic stiffness variation. The simulation result showed instability as expected for the case of using only a standard impedance controller. The behavior over time for the storage function and the position tracking diverges to infinity over time. After implementing the tank algorithm, the system remained stable over time and the position tracking did not diverge from the desired one. To check the robustness of this approach puncturing task experiments were conducted by the authors with tank based algorithm and the results were plotted accordingly.

Another extension of the method that incorporates the principle of energy tanks can be found in [41]. In this approach, they try to develop methods to incorporate the time-varying impedance behavior in the redundant manipulators for both the primary and null space tasks. A passivity-based controller is implemented which uses the concept of energy tanks which are filled by the dissipated power in the system, and it compensates for the non-control passive actions and hence ensures the passivity during free motion and stable interactions with the environment. Since the fact that interconnection of passive subsystem results in passive system in this method the passivity is each system in analyzed independently with respect to its corresponding power port. The passivity is analyzed with the storage function of each subsystem and taking a time derivative of the storage function and verifying if the system shows active behavior. In this case, the primary and the null space task showed active behavior. This was mainly due to the stiffness variation in both the main task controller and null space task controller. And therefore to restore the passivity in the system, the concept of 'energy tanks' is adopted. The main ideology behind this approach is that the tanks allocate a certain amount of energy to the system that could be

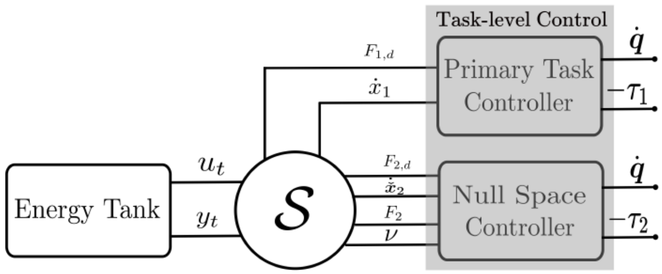

Figure 2.13: Interconnection of Energy Tank with the primary and null space task controllers[41]

used to execute non- passive behavior or control actions. The tanks can also be used to store the energy dissipated by the system (through dampers) and can be reused for ensuring passivity. The energy tanks are interconnected to the primary and null space controllers as shown in the figure 2.13. The tank exchanges energy with the controllers through the power $port(u_t, y_t)$. The primary task controller exchanges energy through the dirac structures through power port $(F_{1,d}, \dot{x_1})$. The energy injected through this port is used to implement stiffness variation in the primary task. $(F_{2,d}, \dot{x_2})$ is used to inject energy necessary to vary the stiffness in the null space task, while the other (F_2, v) compensates for the null space task projection[42] Furthermore, this approach in the simulation where the variable stiffness profile is commanded to both primary and null space tasks. It is shown that with the energy tanks, the system remains passive with the energy always decreasing.

In [43] this article, an argument is made in the terms of linear regression to model human stiffness via EMG signals. The article does show the nearly linear relation between the measured stiffness 'K_h' and the principal component of the measured muscular activation, and it is based on physical measurements of the wrist stiffness. The PCA analysis (principal component analysis) is adopted and an eigenvector is used for the evaluation of muscle activation required to complete a task at hand.
The natural control of the secondary device impedance is estimated via surface electromyography (sEMG) and 1 DOF teleoperation task is conducted to validate this approach the hand stiffness of six healthy subjects was con-

sidered and linearly estimated using the (sEMG) with excellent accuracy (R-square regression coefficients around 0.90). The secondary device impedance was controlled in real-time using the estimated stiffness, which resulted in high precision in position accuracy and contact torques, when the stiffness of high value is commanded. And also force feedback is added to augment the effect of telepresence and control of robotic impedance by human subjects.

Interesting work is done related to the variable model parameters (stiffness) in [44]. Here, the concept of passivity based model updating for the Model Mediated Teleoperation (MMT). In MMT, a simple object model is employed on the main device side to approximate the remote and unseen environment. The main advantage of this approach is that since the haptic control loop will be running locally the system shows stable behavior even in the presence of communication delay. The local model which is present at the main device (or input device) side should be updated whenever the environment changes. Due to this sudden model update or sudden changes in parameters it leads to model or force-jump effects and results in unpredictable motion and hence the system becomes unstable. Therefore to have a smooth and stable model update the concept of passivity-based Model Update (from here on:PMU) is proposed. PMU based approach ensures the stability of local haptic interaction during the model update phase by considering the sampling effect of the haptic device. A 3-D spring-damper model is used to approximate the remote environment, where damping, stiffness, and initial position are considered to be major parameters that would change during the teleoperation. In the coming sections for simplifying the passivity analysis, solutions and methods are provided to overcome instability, that is caused due to the update of stiffness. Considering the stiffness parameter update, increasing the stiffness harms the system passivity. The reason is that, if the stiffness is increased, then consequently energy is generated in the system. If the generated energy is not dissipated by the system damping during the model update phase, the system becomes unstable or non-passive. But whereas for the decreasing stiffness case scenario, this would not be a problem because it would reduce the energy stored in the system, and thus obtains energy for the system passivity. To overcome the effects of increasing stiffness, an additional adaptive damper is designed to achieve system passivity assuming for low-frequency inputs. This adaptive damping element is also used in [22] for the environment with unchanging model parameters.

The performance of the proposed PMU scheme is studied using simulations. At first, the effect of change in stiffness is studied and the results are plotted accordingly.It can be observed that for the case where the PMU method is used the adaptive damping is computed according to [44] and hence the net energy output of the system stays positive. For the case where the PMU method has not been adopted it can be seen that the net energy output of the system decreases to a non-positive value (indicating active behavior) due to stiffness increase. Hence, the results obtained shows that the PMU scheme guarantees the system stability and on the other leads to a more comfortable model update compared to the method that does not adopt this approach.

Chapter 3

Problem statement

3.1 Energetic behavior of variable stiffness

In order to enhance the safe and compliant interaction of the secondary device with the environment, the concept of teleimpedance control can be adapted in the field of teleoperation. Here, the impedance controller of the secondary device adjusts the gains in a similar manner to that of the human arm's despite the delay in the communication channel and enables the user to perform the desired action in an uncertain environment. However, if we consider this situation more carefully, increasing the stiffness in real-time leads to higher kinetic energy generation after the contact with the environment and violates the passivity condition of the bilateral teleoperation system, as the output energy will be higher than the input energy, that eventually makes the system unstable.

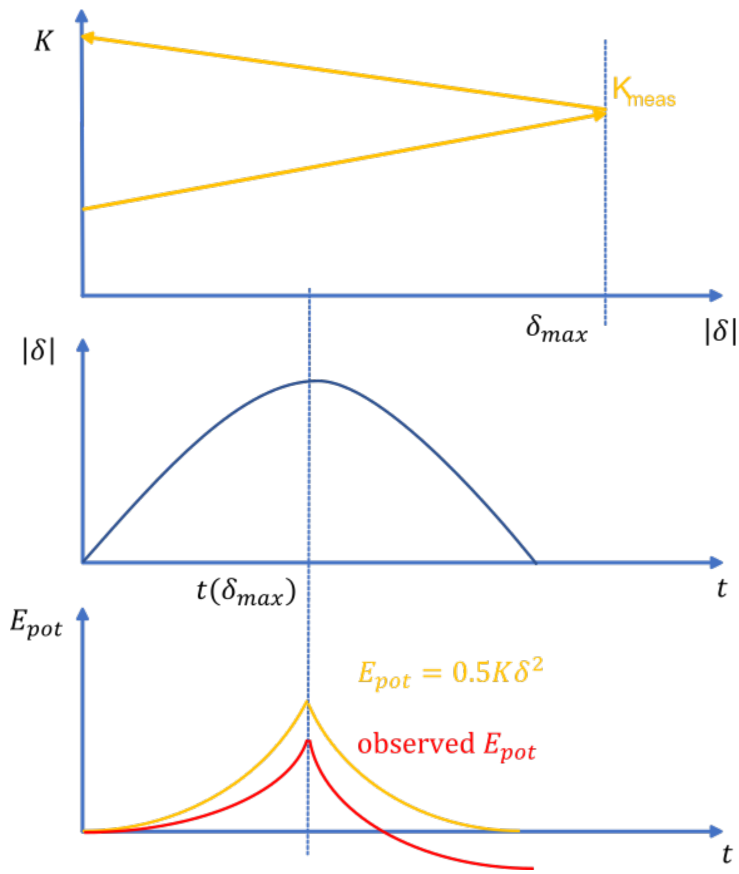

Figure 3.1: Energetic behavior of variable stiffness

The energetic behavior of the system due to variable stiffness can be seen from figure 3.1. The first plot represents the change of stiffness with respect to deflection and for the sake of simplicity, a monotonous increase in stiffness (K_{arm}) is considered. During the pressing phase (when the user makes contact with the object or environment) the value of stiffness increase linearly and reaches a higher value at δ_{max} and due to this the energy in the storage element is charged up as intended by the main and secondary devices, which can be seen in the energy plot where both the observed energy (observed E_{pot}) and the analytically calculated energy (E_{pot}) reaches their peak value at maximum deflection. But in the releasing phase (when the user pulls out contact with an object) if the stiffness continues to increase constantly and reach a higher value at zero deflection ($\delta = 0$) then the observed E_{pot} eventually reaches a non-positive value and this indicates energy generation due to increase in stiffness and thus the system potentially leads to instability. This instability in the system can lead to undesirable effects especially when the secondary device is interacting with the environment. For example, in one of the most critical cases of a narrow passage, and especially in combination with delay, this can lead to a divergent bouncing between two close walls and impacts both the environment and the robot. Therefore the passivity control becomes crucial in this situations.

3.2 Discussion of state-of-the-art method

To accommodate the variable stiffness behavior in the impedance model and assure passivity, the concept of the energy tank approach has been introduced in [39]. This approach has widely been used in the haptics [45] telesurgery [46] and remote insertion and palpation [47]. As explained in the previous sections even though this approach is mathematically accurate, it uses dissipated power to fill up the 'tanks' and is reused for executing potentially non-passive control actions, which is not physically comprehensive. This lacks physical meaning when compared to other mechanical systems, where potential energy (physical energy) is used for storage and has more physical relation to the energy storage element. And also during the steady-state (zero velocity, zero deflection) the energy in the tanks is not reset to its initial conditions as in real mechanical/physical systems [30]. But instead, the energy in the tank is filled up in presence of residual energy from the previous operation.
The storage of energy in the tank takes place only up to a certain limit [48], this because, during ceratin teleoperation mode, the human operator injects a large amount of energy into the system and thus making the stored energy dangerously large. The tanks should have certain threshold energy to deal with variable stiffness behavior. But the value of the threshold that has to be selected or the boundary condition that has to be maintained is not defined. This leads to uncertainty as to how much dissipated energy filled in the tank is required to compensate for the effects of desired variable stiffness and also the forces may be completely canceled by the controller leading to a very low stiffness.

3.3 Implementation of TDPA with variable stiffness

From the figure 3.1 it is proven that implementing variable stiffness causes energy generation within the system, and thus result in active behavior.
To study the effects of stability of the system in the presence of variable stiffness and time delay, the conventional TDPA is subjected to variable stiffness, and simulations were performed in MATLAB and Simulink on a 1-DOF bilateral teleoperation model. For this purpose two types of stiffness variations were considered: A constant increase in stiffness (ramp input) and sinusoidal variation of stiffness. Both these variations were performed in the case of wall contact scenarios. The round trip delay was given in the range of $T_d = 0ms$ to $T_d = 200ms$.

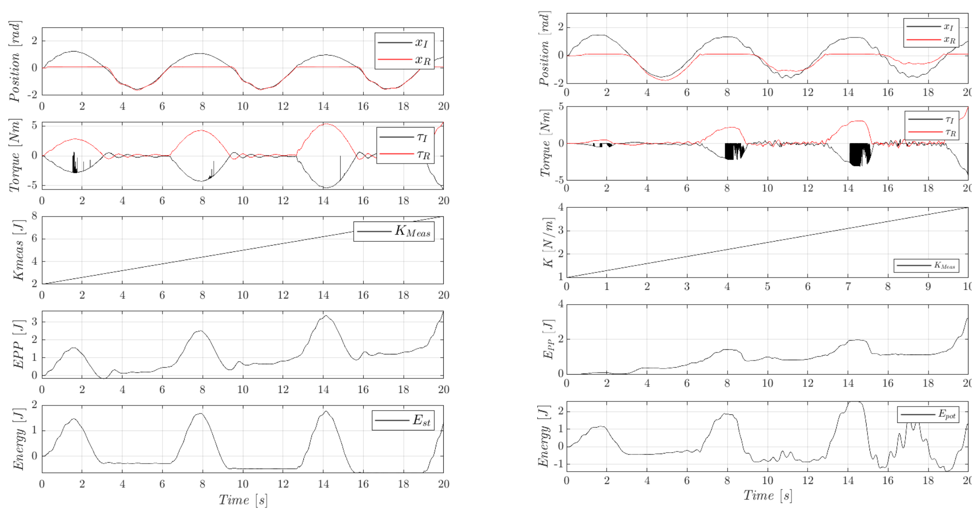

a) No delay (T_d=0ms) round trip **b)** With delay (T_d=200ms) round trip

Figure 3.2: Both a) and b) represents the plots of constant stiffness increase (K_{meas}) in TDPA with wall contact. High frequency PC disturbances towards the main device side can be avoided through the passive filter. It can be seen that for both the cases with and without delay, the net energy output quickly decreases to negative values (the system is active) due to the stiffness increase.

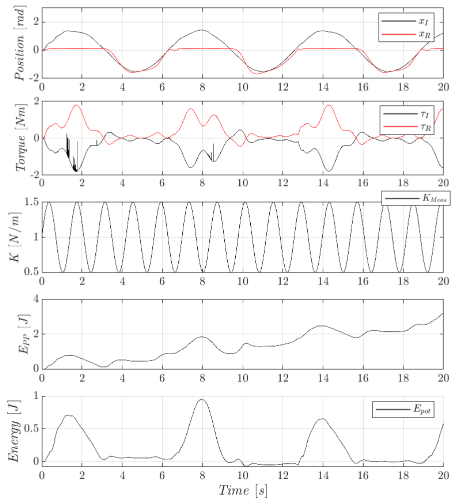

a) No delay (T_d=0ms) round trip

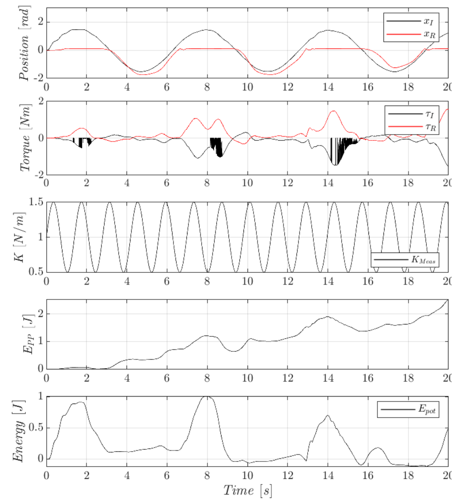

b) With delay (T_d=200ms) round trip

Figure 3.3: Both a) and b) represents the plots of sinusoidal stiffness variation(K_{meas}) in TDPA with wall contact. It can be seen that for both the cases with and without delay,the net energy output decreases to non-positive values. This indicates energy generation in the system due to variable stiffness and potentially leads to instability.

Chapter 4

Proposed control approaches

4.1 TDPA-ER with variable stiffness

The architecture of TDPA-ER with variable impedance is shown as in the figure 4.1

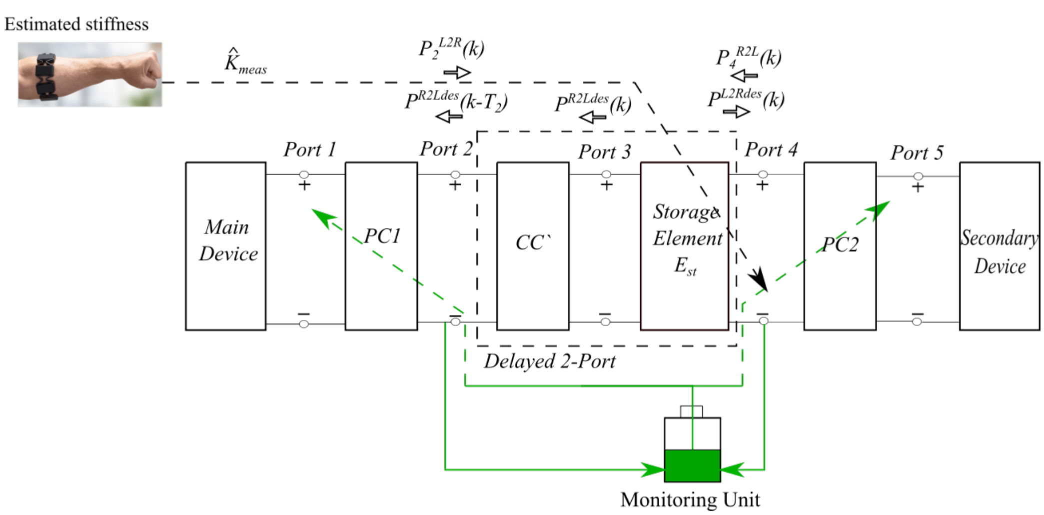

Figure 4.1: TDPA-ER architecture subjected to variable stiffness

Analogous to the other state-of-the-art method, the available amount of

energy is collected in the energy monitoring unit (battery shaped) collecting the energy input from both sides of the delayed 2-port subsystem. Since this monitoring unit has a physical relation to the energy storage element, the monitoring unit is located on the right side of the communication channel and it directly assures passivity of 2-port with variable impedance.
The estimated stiffness parameter (K_h) from the sensor is sent to the coupling controller as shown in the figure 4.1. This method assures passivity since the energy input to the 2-port passivity directly depends upon the variation of the stiffness. And during the releasing phase, the power that leaves the energy storage element at port 3 and port 4 leads to instability since additional energy may be injected due to the increasing or variation in the stiffness in accordance to the user's impedance, these changes could result in non-passive behavior and potentially lead to instability. In order to avoid such issues, the actual output power is limited according to the logic presented in the equation (2.16) and in equation (2.17) in section 2.3 and the desired power $P^{L2R,des}(k)$ and $P^{R2L,des}(k)$ are sent to the main and secondary device side. The excess observed energy is calculated as per the equation (2.18) and(2.19) and this energy will be dissipated by the respective passivity controllers (PC1 and PC2) at each side of the ports. And thus this control approach guarantees system stability and passivity in the presence of variable stiffness.
To examine the behavior of TDPA-ER with variable stiffness, experiments are conducted and the results are plotted accordingly. This will be discussed in the next section.

4.1.1 Results

This state-of-the-art approach of TDPA as explained in section 2.3 was considered as one of the possible solutions in order to solve the problem of variable stiffness.

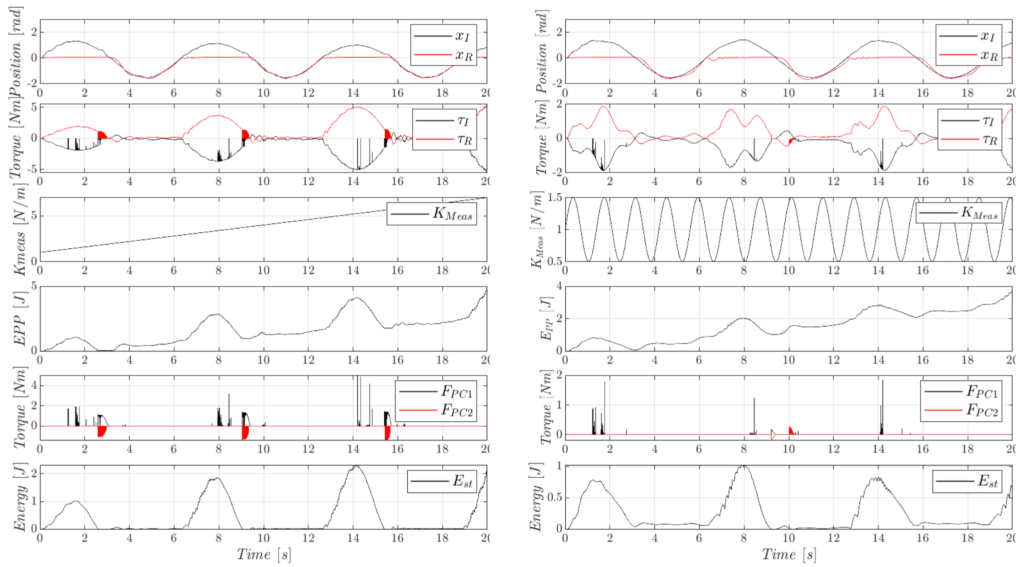

a) Constant increase in stiffness **b)** Sinusoidal variation in stiffness

Figure 4.2: TDPA-ER subjected to variable stiffness under 0ms roundtrip delay

The plots as shown in figure 4.17a and figure 4.2b represents two different types of stiffness variation (K_{Meas}) in TDPA-ER under 0ms roundtrip time delay with wall contact. In figure 4.17a, which is the critical case of stiffness variation the main device force drops suddenly during the releasing path compared to case in figure 4.2b. The position following of the two devices is satisfactory. The charging and releasing of the spring during the two wall contacts (t=[6s,10s] and t = [12.5s,16s]) are visible in the energy plot. Since the E_{PP} never goes negative in this case, the passivity of the system is confirmed.

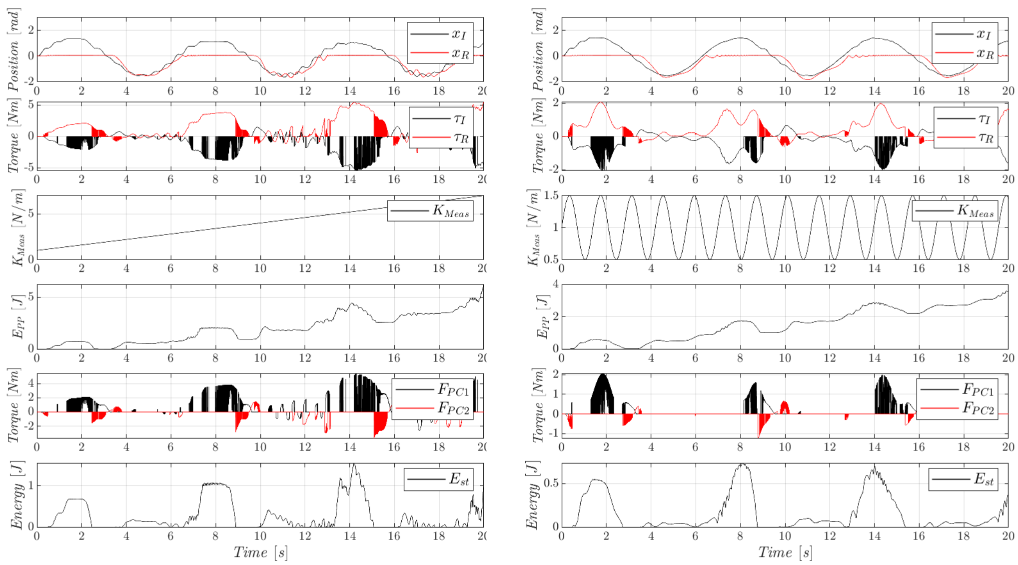

a) Constant increase in stiffness **b)** Sinusoidal variation in stiffness

Figure 4.3: TDPA-ER subjected to variable stiffness under 200ms roundtrip delay

The plots in figure 4.3a and figure 4.3b represents the stiffness variation in TDPA-ER under 200ms time delay with wall contact. In the case of figure 4.3a the main device force drops more rapidly during the releasing path compared to case figure 4.3b. The position following is clearly affected by the high delay. The energy plot (E_{PP}) is always positive and thus confirms the passivity of the PC-controlled network. Due to the impedance type PC force dissipation is higher especially during the wall contact for a constant increase in stiffness than a sinusoidal variation of stiffness. In contrast to conventional TDPA subjected to variable stiffness, no position drift appears despite the high communication delay due to the consideration of energy reflection and the application of impedance-type PCs on both the side.

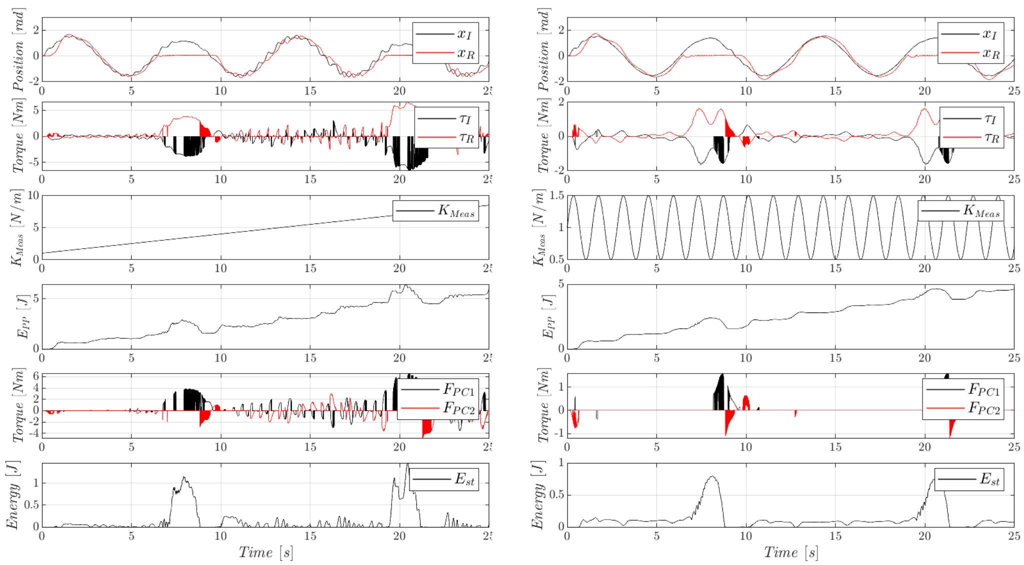

a) Constant increase in stiffness **b)** Sinusoidal variation in stiffness

Figure 4.4: TDPA-ER subjected to variable stiffness under 200ms roundtrip delay with free motion and wall contact.

It can be observed that the main device force drops more rapidly in figure 4.4a than in figure 4.4b during the releasing path. The position following is clearly affected by the high delay. The energy plot (E_{PP}) is always positive and thus confirms the passivity. During free motion less energy needs to be dissipated by the PCs than in wall contact scenarios. Higher force oscillations can be observed during free motion for the constant increase in stiffness (critical case) due to higher time delay. This can be avoided by implementing a low pass filter.

4.1.2 Discussion with drawbacks

The TDPA-ER even though it compensates for the drawbacks of TDPA, it has limitations of its own, if it is subjected to stiffness variation.
The drawbacks of this approach can be examined in the simulation environment, in which a single DOF bilateral teleoperation system is considered with TDPA-ER algorithm. The analysis is done by considering a critical case of

stiffness variations: The constant increase in stiffness (ramp input)
At first, the ramp input (critical case) is considered. When the simulation was conducted for no delay case it can see that the system remains passive i.e the proof of passivity E_{PP} is positive. However, if no energy is available in the storage the force feedback to the main device from the passivity controller drops drastically to zero during the release path, which can be observed by the green area from the plot figure 4.5. This leads to a misinterpretation of the feedback signal by the user. A similar effect can be observed in the case of a time delay of 200ms (round trip) as represented by the green area from the plot figure 4.6 In order to avoid such issues and to prevent secondary device adhering to the wall or environment during the releasing path, the concept of stiffness gradient was introduced to enhance its performance.

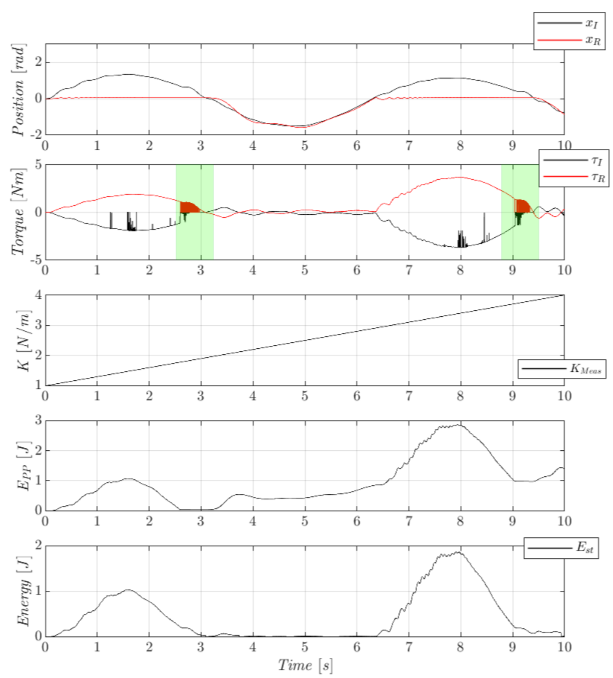

Figure 4.5: The green area represents the sudden force drop on the main device side at no time delay, when the secondary device robot is moving out of the environment (releasing path).

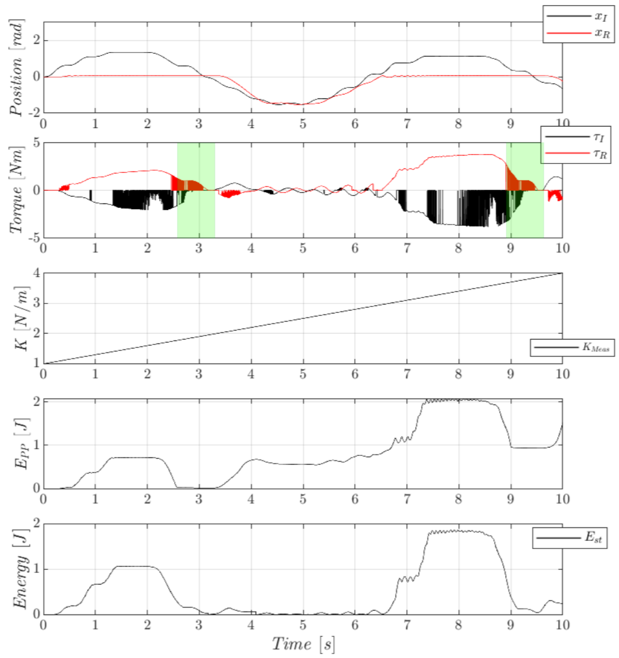

Figure 4.6: The green area represents the sudden force drop on the main device side at a roundtrip delay of 200ms, when the secondary device robot is moving out of the environment (releasing path).

4.2 Gradient Methods

4.2.1 Linear Gradient Concept

To overcome the drawbacks of TDPA-ER and issues regarding variable stiffness the gradient concept was introduced. In the beginning for the sake of simplicity, the linear gradient concept is adopted.

figure 4.7 visualizes the basic idea of the proposed method. It can be observed that during the pressing phase the stiffness from the sensor (in this case monotonous increase in stiffness) is adopted. And due to this the observed energy (E_{pot}) in the storage element that serves the desired coupling behavior is charged up at maximum deflection (δ_{max}) as intended by both the main device and the secondary device. However during the releasing path instead of taking into consideration of stiffness commanded from the sensor(K_{arm}), the passive gradient $\nabla K(k)$ is calculated, which is the function of $\delta(k)$,E_{pot}, K(k) and the allowable stiffness ($K_{allowed}$) obtained from the gradient is adopted. This stiffness reaches a much lower value at zero deflection than compared to K_{arm} and the observed E_{pot} eventually reaches zero unlike the scenario presented in the figure 3.1. This energetic behavior (net observed energy is positive) confirms the passivity in the system without active behavior.

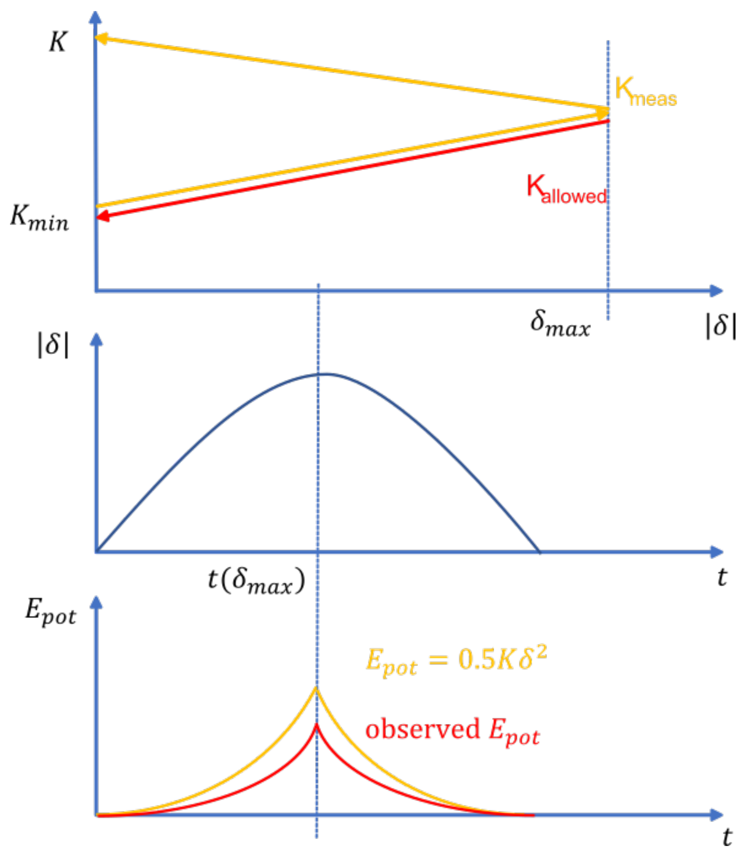

Figure 4.7: Linear gradient concept

In some cases during the release path the $K_{allowed}$ values reaches to zero or negative values in case of constant gradients as it can be seen from the figure 4.8. This makes the system non-passive as observed E_{pot} tends to reach negative values.

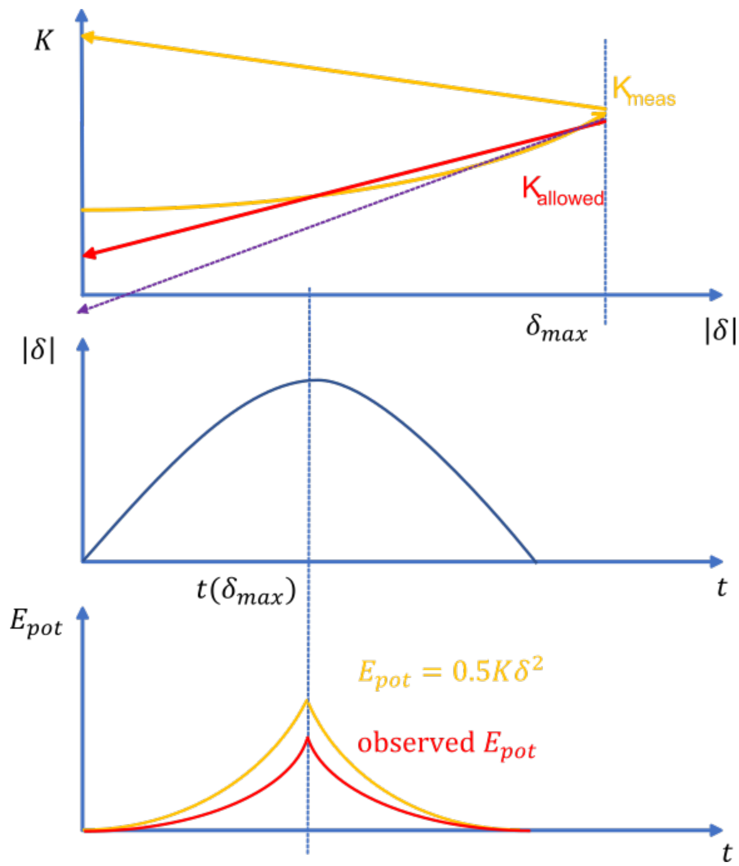

Figure 4.8: Calculated allowable stiffness ($K_{allowed}$) reaching negative values with implementation of linear gradient during releasing path

In order to avoid such issues, the calculated gradient $\nabla K(k)$ on the release path is limited to assure passivity.
A suitable minimum stiffness must be set by the user in order to maintain coupling between the main and the secondary device. This can be obtained by limiting the gradient $\nabla K(k)$ on the pressing path as shown in the figure 4.9 such that a desired minimum stiffness (K_{min}) can be achieved.

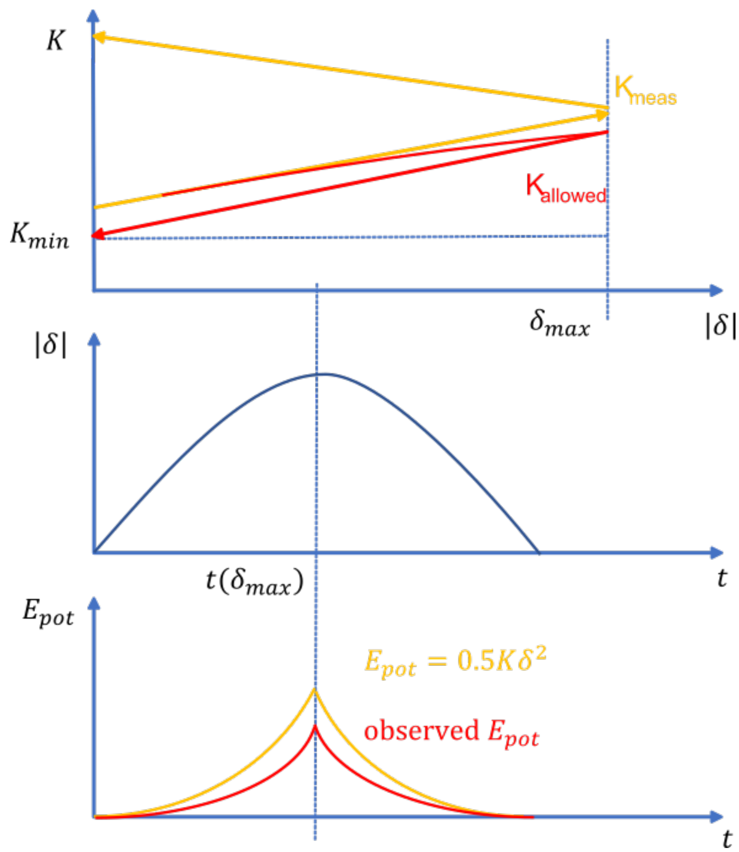

Figure 4.9: Passive Linear gradient both on pressing and releasing path

In contrast to TDPA and other state-of-the-art methods, in this approach, a minimum stiffness 'k_{min}' can be guaranteed at zero deflection assuring position synchronization between the devices. The position drift which used to occur for the conventional TDPA can be avoided if this method is combined with the least conservative approach (TDPA-ER). The behavior of stiffness can be more easily affected with this approach, and thus higher system transparency can be achieved.

Implementation of Linear Gradient

The computation for linear gradient is as shown below:

At time step k, the linear equation ($y = mx + t$) of K with gradient ∇K looks like:

$$\begin{aligned} K(\delta) &= \nabla K(k)\delta + K(k) - \nabla K(k)\delta(k) \\ &= \nabla K(k)(\delta - \delta(k)) + K(k) \end{aligned} \tag{4.1}$$

where δ is the deflection,$\delta(k)$ and K(k) is current deflection and stiffness at time step 'k' respectively and $\nabla K(k)$ is the gradient.

The potential energy at the time step k with deflection $\delta(k)$ and K(k) is:

$$\begin{aligned} E_{pot}(k) &= \int_0^{\delta(k)} K\delta d\delta \\ &= \int_0^{\delta(k)} (\nabla K(k)(\delta - \delta(k)) + K(k))\delta d\delta \\ &= \int_0^{\delta(k)} \nabla K(k)(\delta^2 - \delta(k)\delta) + K(k)\delta d\delta \\ &= \left[\frac{1}{3}\nabla K(k)\delta^3\right]_0^{\delta(k)} - \left[\frac{1}{2}\nabla K(k)\delta(k)\delta^2\right]_0^{\delta(k)} + \left[\frac{1}{2}K(k)\delta^2\right]_0^{\delta(k)} \\ &= \frac{1}{3}\nabla K(k)\delta^3 - \frac{1}{2}\nabla K(k)\delta^3(k) + \frac{1}{2}K(k)\delta^2(k) \\ &= \nabla K(k)(\frac{2}{6} - \frac{3}{6}\delta^3(k) + \frac{1}{2}K(k)\delta^2(k) \end{aligned} \tag{4.2}$$

Solve for $\nabla K(k)$ we get:

$$\nabla K(k) = \frac{-6(E_{pot}(k) - \frac{1}{2}K(k)\delta^2(k)}{\delta^3(k)} \tag{4.3}$$

This calculated $\nabla K(k)$ gradient acts as a passive gradient for both the pressing and release path. Both this passive gradients limits the measured gradient ∇K_{meas} (gradient of stiffness obtained from the sensor) such that the system would remain passive with variable stiffness. The allowed stiffness ($K_{allowed}$) can be obtained from this computed gradient by integrating it with respect to deflection ($\delta(k)$). The stiffness at zero deflection can be calculated with the help of gradient using the equation

$$K_{zero} = K(k) + \nabla K(k) * \delta(k) \tag{4.4}$$

If the value of stiffness (K_{zero}) is lower than or equal to minimum stiffness then the gradient on the pressing path has to be limited.
To understand the behavior of the linear stiffness gradient control, The simulations were performed in Simulink by taking two input sine wave signals as shown in the figure 4.10 which represents the position of the main device (input device) and secondary device (output device). The signal of the main device has an amplitude of 1 and frequency of 3 rad/sec and the secondary device has an amplitude of 0.9 and frequency of 3 rad/sec and for the sake of analysis two different types of stiffness variations were considered: The constant increase in stiffness (ramp input) and sinusoidal variation of stiffness.

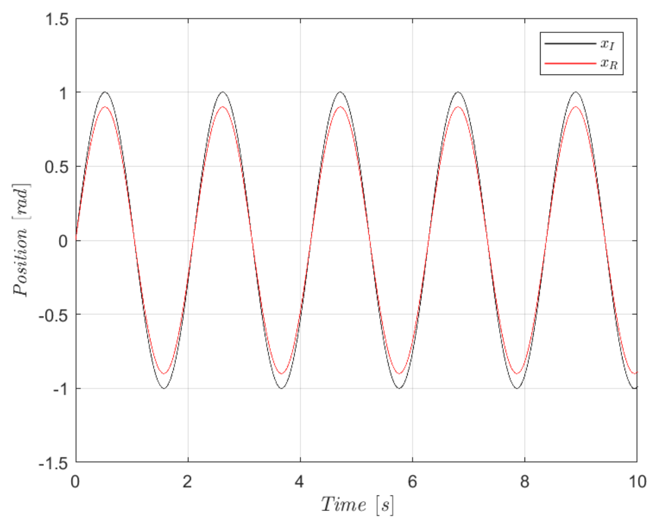

Figure 4.10: Position signals for main and secondary device

The graph of Stiffness vs deflection is plotted as shown in the figure 4.11 and figure 4.12

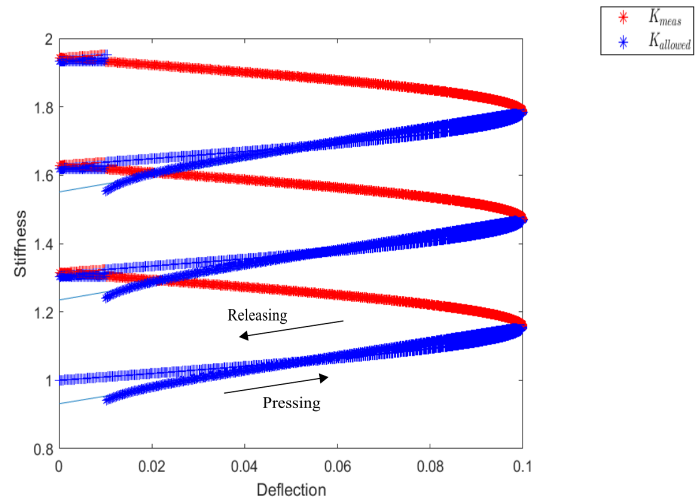

Figure 4.11: The plot of stiffness vs deflection with the implementation of linear gradient for ramp input (constant increase in stiffness. K_{meas} represents the estimated stiffness input and K_{allow} indicates the allowable stiffness obtained from the passive gradient.

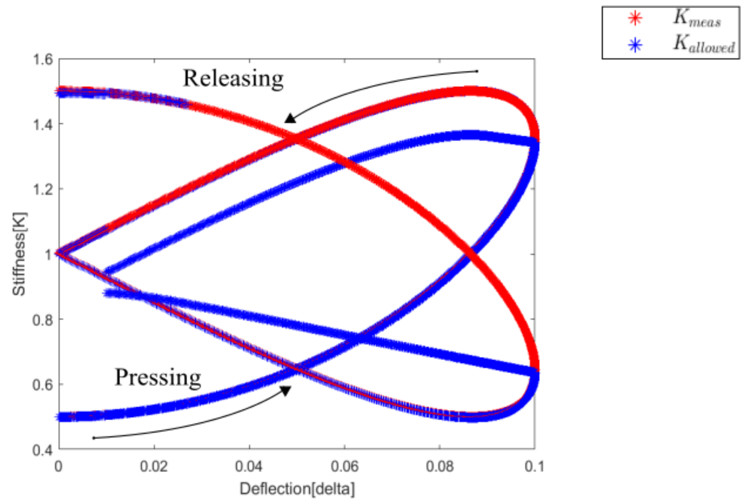

Figure 4.12: The plot of stiffness vs deflection with the implementation of linear gradient for sinusoidal input. K_{meas} represents the estimated stiffness (sinusoidal variation in stiffness in this case) and K_{allow} indicates the allowable stiffness obtained from the calculated passive gradient that assures passivity.

As it can be seen from the plot the red line represents the desired stiffness (K_{des}) commanded from the sensor, but here in this analysis case, we take the most critical case, which is a ramp input. And the blue line represents the allowed stiffness ($K_{allowed}$). It can be seen that the (K_{allow})follows the (K_{des}) line during the pressing phase and the releasing phase the ($K_{allowed}$)drops linearly and hence showing that this is the allowed stiffness that is required to maintain passivity. Similarly, even in the case of sinusoidal stiffness input, it can be seen that in the figure 4.12 during the releasing path the (K_{allow}) drops linearly in order to assure passivity and compensate for the energy generation that occurred during the increase in stiffness phase.
It is important to note that in contrast to other state-of-the-art method, in this approach the passive stiffness (K_{allow}) is reset back to initial conditions (K_{meas}) during zero deflection or free-motion as in the case of real physical systems.

Discussion with drawback

One of the drawbacks of this approach is that the desired K_{min}, which is necessary for position synchronization between the devices is not always set and it has to be manually set by the user during the operation. This approach gave better results in the simulations than compared to its implementation on experiments(1-DOF device). During the experiment, the stiffness K_{allow} during the releasing path becomes negative due to the linear gradient and thus resulting in drastically changing the coupling behavior between the devices. In order to avoid such drawbacks, a new Non-linear gradient method was developed and its concept and implementation will be explained in the next section.

4.2.2 Non-linear Gradient Concept

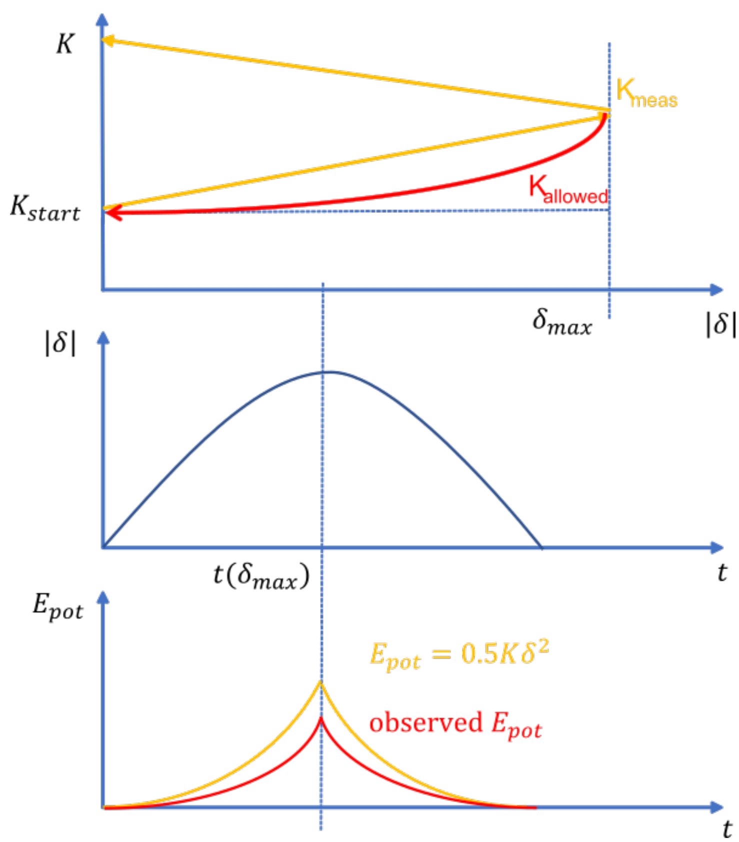

Figure 4.13: Non-linear gradient concept. The first plot represents stiffness vs deflection, where K_{start} is the initial value of stiffness at the start of pressing phase, when $\delta \approx 0$, $K_{allowed}$ is the allowable stiffness and K_{start} is the estimated stiffness from sensor. The second plot shows the variation of deflection over time and the third plot denotes the variation of potential energy (E_{pot}) over time.

The concept of Non-linear gradient can be seen in figure 4.13. similar to the previous case monotonous increase in stiffness (critical case) is assumed for the sake of simplicity. During the pressing phase, it can be seen that the stiffness increases constantly(K_{arm}) from K_{start} and reaches a higher value at maximum deflection δ_{max}. Due to this, the energy in the storage element is charged up, as it can be seen from the plot where observed (E_{pot}) curve increase until maximum deflection (δ_{max}) is attained. However, during the releasing phase the passive Non-linear gradient $\nabla K(k)$ is calculated, which is the function of $\delta(k)$,E_{pot}, K(k) and the allowable stiffness($K_{allowed}$) obtained from the gradient is adopted. In contrast to the previous approach it can be observed that the stiffness $K_{allowed}$ drops in a manner of the parabolic curve and reaches approximately to the same value of K_{start}. This eliminates force jumps in the system and the $K_{allowed}$ does not reach negative values in the case of the non-linear gradient. The charged-up energy in the storage element is released to the system during the releasing phase, which is indicated in the plot where observed (E_{pot}) drops and eventually reaches zero. This energetic behavior (net observed energy is positive) confirms the passivity in the system without active behavior.

Implementation of Nonlinear Gradient

The implementation of Non-linear gradient concept is as follows: At time step k, the polynomial equation ($y = ax^d + bx + c$) of K with gradient ∇K can look like:

$$K(\delta) = a(\delta)^d + b(\delta) + c. \tag{4.5}$$

We skip further polynomial parts for simplicity in the beginning. The most effective parameter in the polynomial is the exponent 'd' which has the biggest effect on the non-linearity of the curve. The minimal value of $d \geq 1$ has to be found for which K_{min} can be reached. The parameters a to c have to be determined according to the respective d, K(k), $\delta(k)$, E_{pot} and the following conditions:
At $\delta = 0$, the K(0) should be close to K_{start}.

$$K(0) = c \approx K_{start}. \tag{4.6}$$

K_{start} is the K(k) when starting the pressing at $\delta \approx 0$
$K(\delta(k)) = K(k)$ is another condition, when starting the releasing phase at δ_{max}

$$K(k) = a\delta^d(k) + b\delta(k) + K_{min}. \tag{4.7}$$

$$K(k) - K_{min} - b\delta(k) = a\delta^d(k). \tag{4.8}$$

if d=2, a linear solution according to the previous section should be searched to allow for the negative slopes.

$$\begin{aligned} E_{pot}(k) &= \int_0^{\delta(k)} .K(k)\delta d\delta \\ &= \int_0^{\delta(k)} a\delta^{d+1} + b\delta^2 + c\delta d\delta \\ &= \left[a\frac{1}{d+2}\delta^{d+2}\right]_0^{\delta(k)} + \left[b\frac{1}{3}\delta^3\right]_0^{\delta(k)} + \left[c\frac{1}{2}\delta^2\right]_0^{\delta(k)} \\ &= a\frac{1}{d+2}\delta^{d+2}(k) + b\frac{1}{3}\delta^3(k) + c\frac{1}{2}\delta^2(k). \end{aligned} \tag{4.9}$$

This equation can be solved for 'b':

$$E_{pot}(k) - a\tfrac{1}{d+2}\delta^{d+2}(k) - c\tfrac{1}{2}\delta^2(k) = b\tfrac{1}{3}\delta^3(k).$$

$$b = \frac{E_{pot}(k) - \frac{a}{d+2}\delta^{d+2}(k) - \frac{c}{2}\delta^2(k))}{\frac{1}{3}\delta^3(k)}. \tag{4.10}$$

K(k) can be calculated by Fusing (4.7) and (4.9), we get:

$$K(k) - c - b\delta(k) = a\delta^d(k).$$

$$b = \tfrac{E_{pot}(k) - \frac{a}{d+2}\delta^{d+2}(k) - \frac{c}{2}\delta^2(k))}{\frac{1}{3}\delta^3(k)}.$$

$$K(k) - c - \tfrac{E_{pot}(k) - \frac{a}{d+2}\delta^{d+2}(k) - \frac{c}{2}\delta^2(k))}{\frac{1}{3}\delta^3(k)}\delta(k) = a\delta^d(k).$$

$$K(k) - c - \tfrac{E_{pot}(k) - \frac{c}{2}\delta^2(k)(k))}{\frac{1}{3}\delta^3(k)}\delta(k) + \tfrac{\frac{a}{d+2}\delta^{d+2}(k)}{\frac{1}{3}\delta^3(k)\delta(k)} = a\delta^d(k).$$

$$K(k) - c - \frac{E_{pot}(k) - \frac{c}{2}\delta^2(k)(k))}{\frac{1}{3}\delta^3(k)}\delta(k) + a\frac{\delta^{d+2}(k)}{\frac{1}{3}\delta^3(k)(d+2)}\delta(k) = a\delta^d(k).$$

$$K(k) - c - \frac{E_{pot}(k) - \frac{c}{2}\delta^2(k)(k))}{\frac{1}{3}\delta^3(k)}\delta(k) = a(\delta^d(k) - \frac{\delta^{d+2}(k)}{\frac{1}{3}\delta^3(k)(d+2)}\delta(k)).$$

$$a = \frac{K(k) - c - \frac{E_{pot}(k) - \frac{c}{2}\delta^2(k)(k))}{\frac{1}{3}\delta^3(k)}\delta(k)}{(\delta^d(k) - \frac{\delta^{d+2}(k)}{\frac{1}{3}\delta^3(k)(d+2)}\delta(k))}.$$

$$a = \frac{K(k) - c - \frac{3E_{pot}(k) - \frac{3c}{2}\delta^2(k)}{\delta^2(k)}}{(\delta^d(k))(1 - \frac{3}{d+2})}.$$

$$a = \frac{K(k) - c - \frac{3E_{pot}(k)}{\delta^2(k)} - \frac{3c}{2}}{(\delta^d(k))(1 - \frac{3}{d+2})}. \tag{4.11}$$

Now substitute the value of value of ‘a’ and ‘b’ in the first equation (4.6). Thus, K(k) becomes

$$K(k) = c - \frac{(\delta^d(c - Kk + \frac{(3Epot - \frac{3c\delta(k)^2)}{2}}{\delta(k)^2}}{(\delta(k)^d - \frac{(3\delta(k)^{d+2})}{(\delta(k)^2(d+2)))}}$$
$$+ (3\delta(Epot - \frac{c\delta(k)^2}{2} + (\delta(k)^{(d+2)}(c - Kk + \frac{(3Epot - \frac{(3*c\delta(k)^2)}{2})}{deltak^2))}}{((\delta(k)^d - \frac{\frac{(3deltak^(d+2))}{(\delta(k)^2(d+2)))*(d+2))))}}{\delta(k)^3}}). \tag{4.12}$$

According to the equation (4.6) substitute K_{start} in the place of ‘c’ as it represents the value of stiffness(K(k))during the starting of pressing at $\delta \approx 0$

$$K(k) = K_{start} - \frac{(\delta^d(K_{start} - Kk + \frac{(3Epot - \frac{3K_{start}\delta(k)^2)}{2}}{\delta(k)^2}}{(\delta(k)^d - \frac{(3\delta(k)^{d+2})}{(\delta(k)^2(d+2)))}}$$
$$+ (3\delta(Epot - \frac{K_{start}\delta(k)^2}{2} + (\delta(k)^{(d+2)}(K_{start} - Kk + \frac{(3Epot - \frac{(3K_{start}\delta(k)^2)}{2})}{deltak^2))}}{((\delta(k)^d - \frac{\frac{(3deltak^(d+2))}{(\delta(k)^2(d+2)))*(d+2))))}}{\delta(k)^3}}) . \tag{4.13}$$

The gradient of this function$\nabla K(k)$ can be calculated with respect to deflection and is given by:

$$\nabla K(k) = \frac{(3*(Epot - \frac{(Kstart*\delta(k)^2)}{2} + \frac{(\delta(k)^{(d+2)}*(Kstart-Kk+\frac{(3*(Epot-\frac{(Kstart*\delta(k)^2)}{2}}{\delta(k)^2}}{((\delta(k)^d-\frac{(3*\delta(k)^{(d+2)})}{(\delta(k)^2*(d+2)})})*(d+2))))}{\delta(k)^3}.$$
$$-\frac{d\delta^{d-1}*(Kstart-Kk+\frac{(3*(Epot-\frac{(Kstart*\delta(k)^2)}{2}))}{\delta(k)^2}}{(\delta(k)^d-\frac{(3*\delta(k)^{(d+2)})}{(\delta(k)^2*(d+2))}}. \tag{4.14}$$

Similar to the previous implementation figure 4.10 to understand the behavior of the non-linear stiffness gradient controller, the simulations is performed in simulink by taking two input sine wave signals which represents the positions of main device (input device) and secondary device (Output device). Two different types of stiffness variations are considered: Constant increase in stiffness (ramp input) and sinusoidal variation of stiffness.
The graph of Stiffness vs deflection is plotted as shown in the figure 4.14

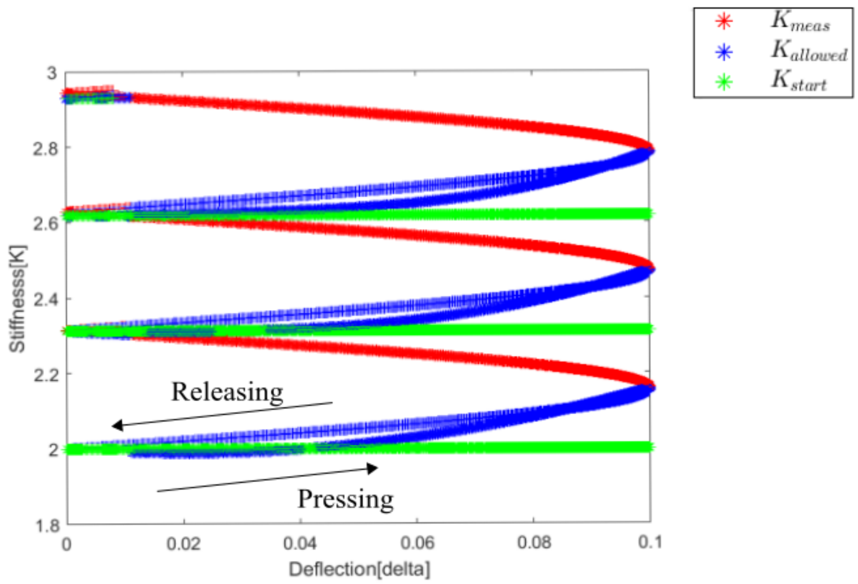

Figure 4.14: The Plot of Stiffness vs Deflection with the implementation of non-linear gradient for ramp input (constant increase in stiffness)

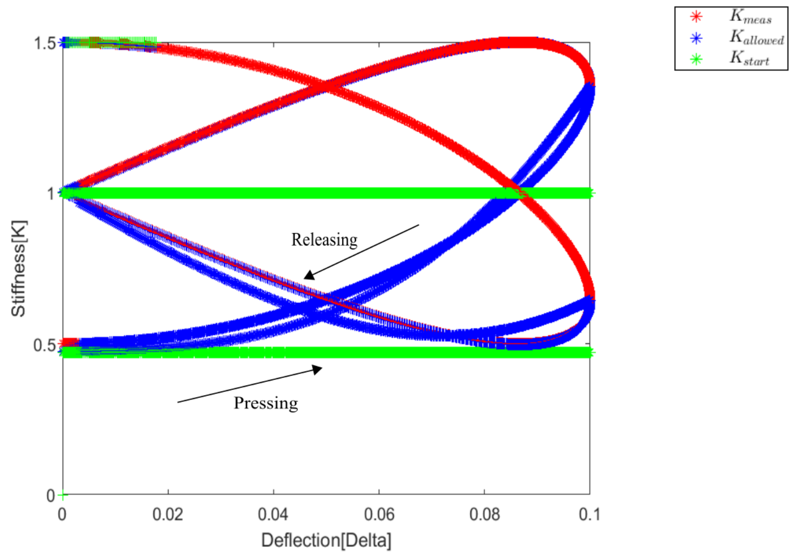

Figure 4.15: The Plot of Stiffness vs Deflection with the implementation of non-linear gradient for sinusoidal input

At first, the analysis is done for the ramp input (constant linear increase) case. As it can be observed from the figure 4.14, The green line in the plot represents the value of K_{start} which indicates the stiffness at $\delta \approx 0$. It remains constant for one complete cycle of the pressing and release phase. The red line in the plot is the value of K_{Des}. This line initiates from K_{start} and increases during the pressing path(when deflection δ goes from 0 to 0.1) and reaches a higher value than the initial value (K_{start}) during the releasing path (when deflection δ goes from 0.1 to 0). This leads to higher energy generation in the system and leads to instability if this desired stiffness is adopted. Therefore the allowable or passive stiffness (K_{allow}) is computed based on the non-linear gradient equation as shown before. The purple line in the plot shows the value of K_{allow}. It can be seen that the K_{allow} follows the K_{des} line during the pressing phase and during the releasing path it drops in a non-linear manner and reaches a value below or equal to the K_{start}

based on the degree of polynomial adopted. Similarly, the analysis is done for Sinusoidal variation of stiffness as shown in the figure 4.15. And hence implementing this method satisfies the passivity condition as there would not be excess energy generation or high force feedback to the user.

Discussion

This proposed gradient concept overcomes the limitations of the previous approach and its effectiveness can be analyzed in further sections. During the releasing path the allowable stiffness (K_{allow}) reaches to the point of initial stiffness (K_{start}) and therefore, the minimum stiffness that is required to maintain the position synchronization between the devices is maintained and thus prevents the user from setting the desired stiffness for each operation.

4.3 Passive Time-Delayed Teleoperation with variable Impedance

4.3.1 TDPA-ER with Nonlinear Gradient

Taking into consideration the disadvantages of TDPA-ER as discussed in the previous section, The combination of the least conservative approach (TDPA-ER) and stiffness gradient concept was implemented.
Implementing of Linear gradient concept with TDPA-ER did not seem to be a suitable choice because of its drawback as mentioned in the previous section and its unresolved challenges in the experiment. So therefore the Non-linear gradient concept was an appropriate choice to combine it with the TDPA-ER.
The architecture is arranged as shown in the figure 4.16.

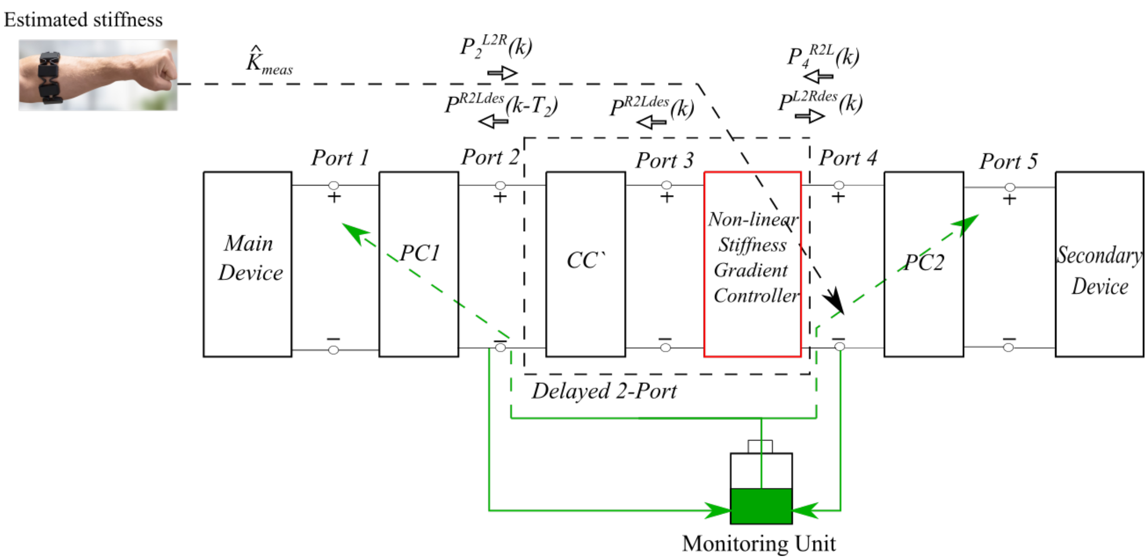

Figure 4.16: The proposed architecture TDPA-ER combined with Non-linear stiffness Gradient controller subjected to variable stiffness estimated from the EMG hardware

The two impedance type passivity controllers (PC) are located on either side of the communication channel (CC) in order to consider the energy storage element together with the CC in 2-port delayed network. The monitoring unit is located at the right side of the communication channel as shown in the figure 4.16.
The stiffness estimation is done by EMG hardware with 8 channels of sEMG electrodes attached to the human arm. In order to deal with the variable stiffness behavior, the coupling controller that is normally used in previous approaches is replaced by a nonlinear gradient controller. This is necessary because of the following reasons: To ensure passivity, reduce the force feedback to the user, and overcome the drawbacks of TDPA-ER in case of variable stiffness.
The stiffness (K_{meas}) is commanded from the sensor to the stiffness gradient controller and the K_{des} is computed as :

$$\nabla K_{Des} = \frac{\partial K_{Des}}{\partial \delta} = \left(\frac{\partial K_{Meas}}{\partial T}\right)/\left(\frac{\partial \delta}{\partial T}\right).$$

$$\frac{\partial K_{Des}}{\partial T} = \left(\frac{\partial K_{Des}}{\partial \delta}\right) * \frac{\partial \delta}{\partial T}.$$

$$K_{des} = \int \nabla K_{des} * dt. \tag{4.15}$$

where ∇K_{Des} is the desired stiffness gradient and K_{Des} is the desired stiffness.
During the pressing path the desired stiffness K_{Des} is achieved but during the releasing path i.e when the main device retrieves from the wall contact, The nonlinear gradient is computed as derived in the previous section.

$$\nabla K(k) = \frac{(3 * (Epot - \frac{(Kstart*\delta(k)^2)}{2} + \frac{(\delta(k)^{(d+2)} * (Kstart - Kk + \frac{(3*(Epot - \frac{(Kstart*\delta(k)^2)}{2}}{\delta(k)^2}}{((\delta(k)^d - \frac{(3*\delta(k)^{(d+2)})}{(\delta(k)^2*(d+2)}))*(d+2))))}}{\delta(k)^3}.$$
$$- \frac{d\delta^{d-1} * (Kstart - Kk + \frac{(3*(Epot - \frac{(Kstart*\delta(k)^2)}{2}))}{\delta(k)^2}}{(\delta(k)^d - \frac{(3*\delta(k)^{(d+2)})}{(\delta(k)^2*(d+2))}}. \tag{4.16}$$

The minimal value of $d \geq 1$ has to be found for which K_{min} value can be obtained. The parameters K(k), $\delta(k)$, E_{pot} represents the current stiffness, deflection and potential energy respectively at the time instant k.
In order to ensure the passivity, the switching up of the gradient takes place. During the pressing path, the desired gradient from the sensor is adopted and during the releasing path, this desired gradient is limited by the calculated passive gradient.
The allowable stiffness is calculated K_{allow} from this gradient:

$$K_{allow} = \int \nabla K(k) * d\delta. \tag{4.17}$$

the stiffness thus obtained drops in a non-linear manner as explained in plots in the upcoming section.
The force commanded 'F_{cd}' from the stiffness gradient controller to the main and secondary device is given by:

$$F_{cd} = K_{allow} * \delta. \tag{4.18}$$

.

Results

This section comprises simulation results obtained from MATLAB and Simulink. The goal of the following simulation is to test the stability of the system during the implementation of variable stiffness. In particular, the desired stiffness, which is provided to the system was chosen to be: constant increase in stiffness (ramp input) and sinusoidal stiffness variation. The time delay in the communication channel is chosen from 0ms to 200ms round trip.
In order to overcome the drawbacks of the energy reflection TDPA the concept of Non-linear gradient was introduced and is computed as shown in the previous section. The traditional coupling controller is replaced with the non-linear gradient controller as shown in the figure 4.16. The simulation results are plotted for this approach, considering different possible cases. The plot of stiffness vs deflection is also shown in order to analyze the stiffness behavior throughout the operation.

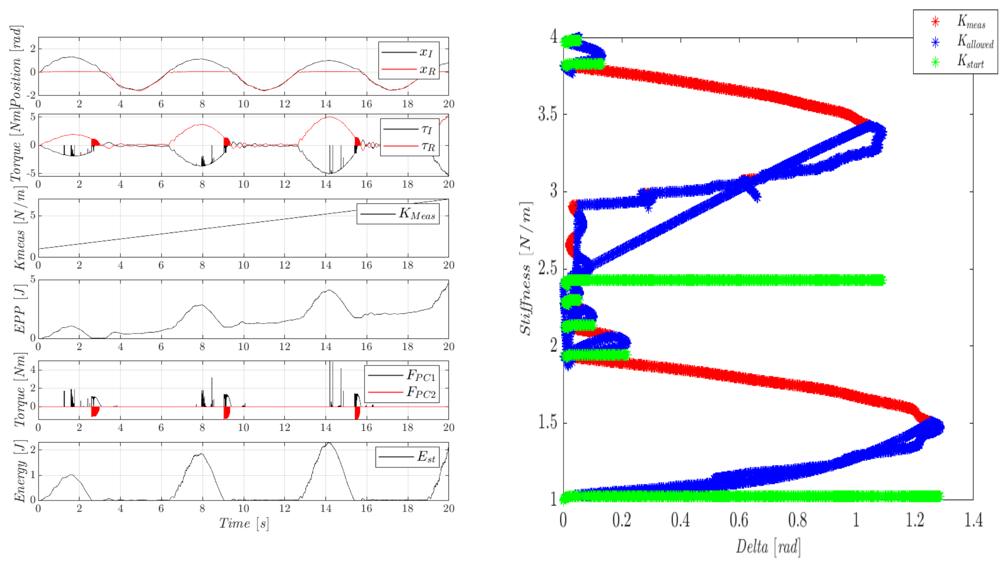

a) Constant increase in stiffness. **b)** Plot of Stiffness vs Deflection.

Figure 4.17: TDPA-ER with Nonlinear gradient subjected to variable stiffness under no delay with wall contact.

figure 4.17a represents stiffness variation in TDPA-ER with Non-linear gradient. In contrast to TDPA-ER method the sudden dropping of main device force is absent during the releasing path. figure 4.17b indicates the behavior of the stiffness during the operation. During the pressing path the passive stiffness K_{allow} follows K_{des} but during releasing path it drops in a nonlinear manner and reaches K_{start}. In contrast to linear gradient concept a minimum position synchronization can be maintained between the devices during all the cases (minimum stiffness can be guaranteed at zero deflection). The energy plot (E_{PP}) is always positive and thus confirms the passivity of the PC controlled network.

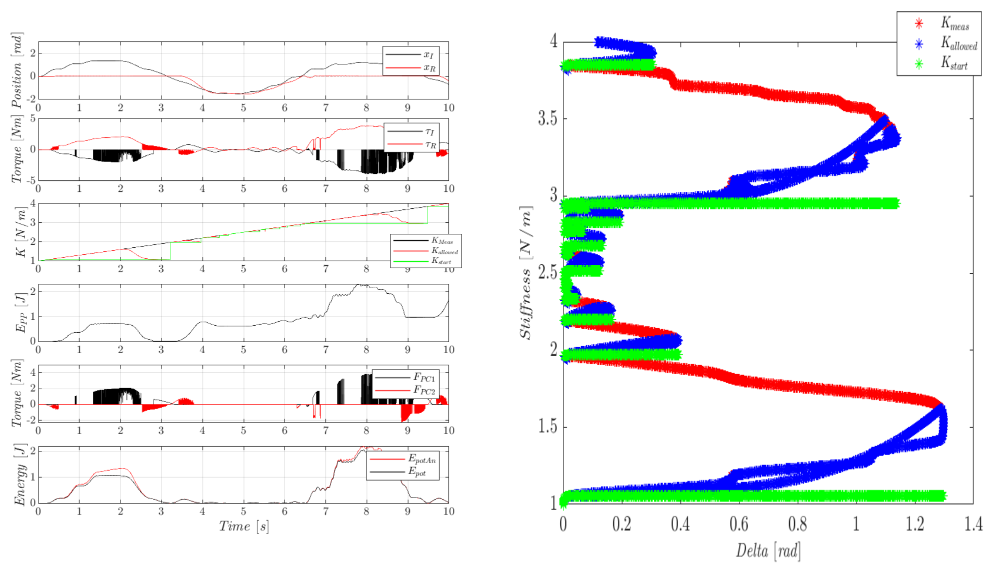

a) Constant increase in stiffness **b)** Plot of Stiffness vs Deflection.

Figure 4.18: TDPA-ER with nonlinear gradient subjected to variable stiffness under 200ms roundtrip delay with wall contact.

figure 4.18a represents stiffness variation (ramp input) in TDPA-ER with Non-linear gradient. The position tracking between the device is clearly affected due to higher time delay. The position drift does not occur despite high communication delay. This combination of Non-linear gradient controller, enables eliminate the high frequency force vibrations on the main device side. Mainly PC1 (PC at main device side) dissipates higher energy during the wall contact. In contrast to TDPA-ER method rapid force drops during the releasing path cannot be observed .The energy plot (E_{PP}) and the net observed potential energy (E_{pot}) is always positive and thus confirms the passivity of the system. The plot presented in figure 4.18b represents the stiffness behavior. The dropping of passive stiffness K_{allow} in a non-linear or parabolic manner can be clearly observed at higher deflection during the releasing path.

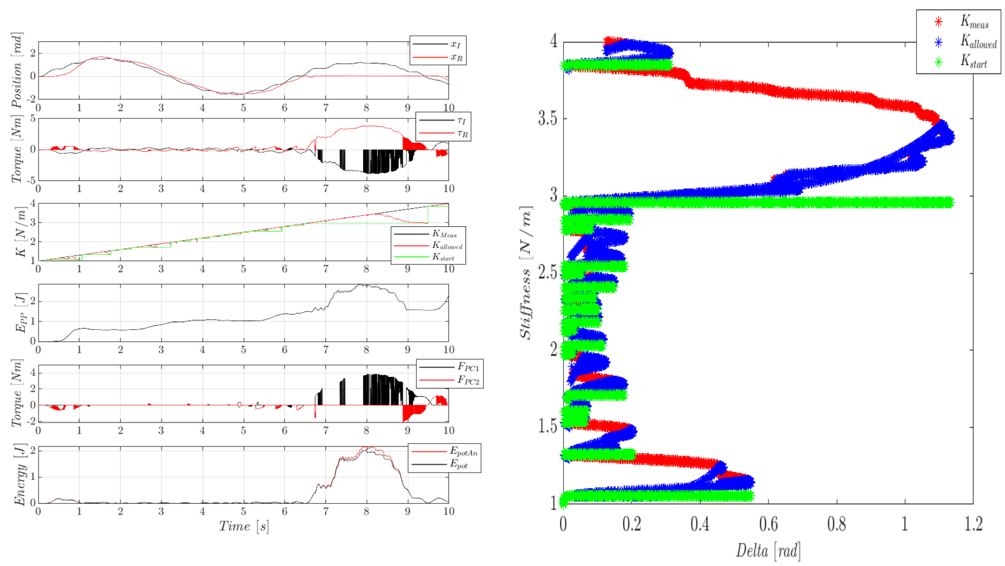

a) Constant increase in stiffness. **b)** Plot of Stiffness vs Deflection.

Figure 4.19: TDPA-ER with nonlinear gradient subjected to variable stiffness under 200ms roundtrip delay with free motion and wall contact.

In figure 4.19a it can be seen that PC forces generated during wall contact are high compared to free motion. The position tracking is normally affected due to high delay but the position drift does not occur. In contrast to TDPA-ER at higher delay this approach has less force drops during the releasing path. E_{PP} remains positive and thus the passivity of the system is confirmed.

Discussion

The results shown in the previous section indicate the effectiveness of the Non-linear gradient concept combined with TDPA-ER. The position-synchronization is slightly affected in case of higher time delay, but the position drift does not occur in all cases. The feedback force is not cut off rapidly during the releasing path as observed in the previous case (only TDPA-ER), this ensures higher transparency in the system. The proof of passivity E_{PP} remains positive and thus the passivity of the system is confirmed for all the considered stiffness variation cases.

4.3.2 TDPA with Nonlinear Gradient

In the case of conventional TDPA it can be seen that, if variable stiffness is implemented, the system tends to go non-passive and results in instability. To avoid this the concept of stiffness gradient control can be implemented in order to accommodate for non-passive actions resulting from variable stiffness. The linear gradient concept for this case scenario seemed unfeasible because of the drawbacks as mentioned in the previous section. Therefore the principle of the non-linear gradient is adopted.
The architecture of TDPA with non-linear gradient control is as shown in the figure 4.20

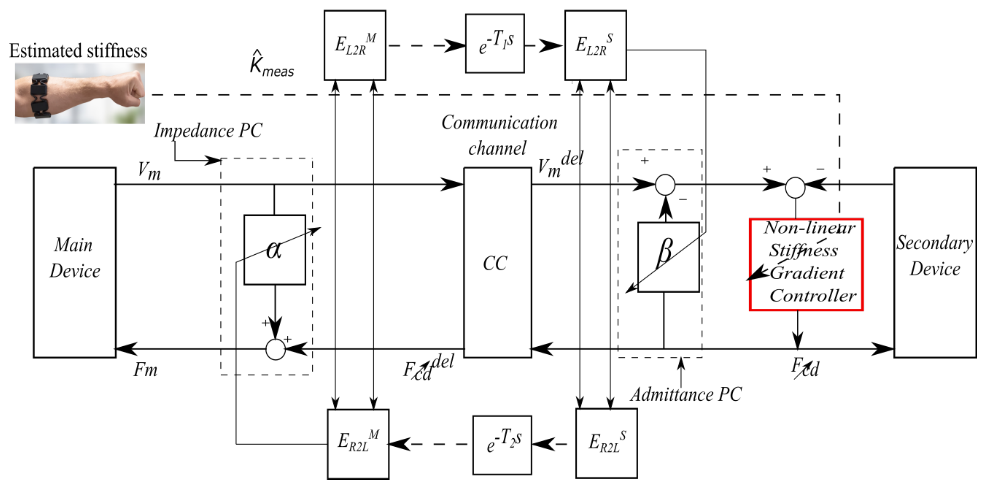

Figure 4.20: The proposed architecture of standard TDPA combined with Non-linear Stiffness Gradient controller subjected to variable stiffness estimated from the EMG hardware.

The position controller that was present in the previous conventional model is replaced by the stiffness gradient controller in order to adapt with variation in stiffness. The impedance passivity controller is placed towards the left side of the communication channel (CC) and the admittance type passivity control is placed at the right side of the CC before the stiffness gradient controller. The PCs present on either side provide delay compensation and removes excess energy generated in the communication channel due to the time delay. The stiffness of the arm muscle is estimated from the EMG hardware is sent to the controller. The Non-linear gradient controller works similarly as explained in the previous section. The desired stiffness is achieved during the pressing path or when the secondary device comes in contact with the object or environment. This is very much essential so that the required task can be accomplished with ease and position accuracy can be achieved. And during the releasing path due to the calculated passive gradient, the allowable stiffness can be calculated and interaction forces can be reduced which demonstrates a better performance, regardless of the delay in the communication channel, while still satisfying the passivity condition.

Results

This approach of Non-linear Stiffness Gradient is adopted to the traditional TDPA in order to assure passivity in the case of variable stiffness. The simulation results are plotted for this approach, considering different possible cases and the plot of stiffness vs deflection is also shown accordingly .

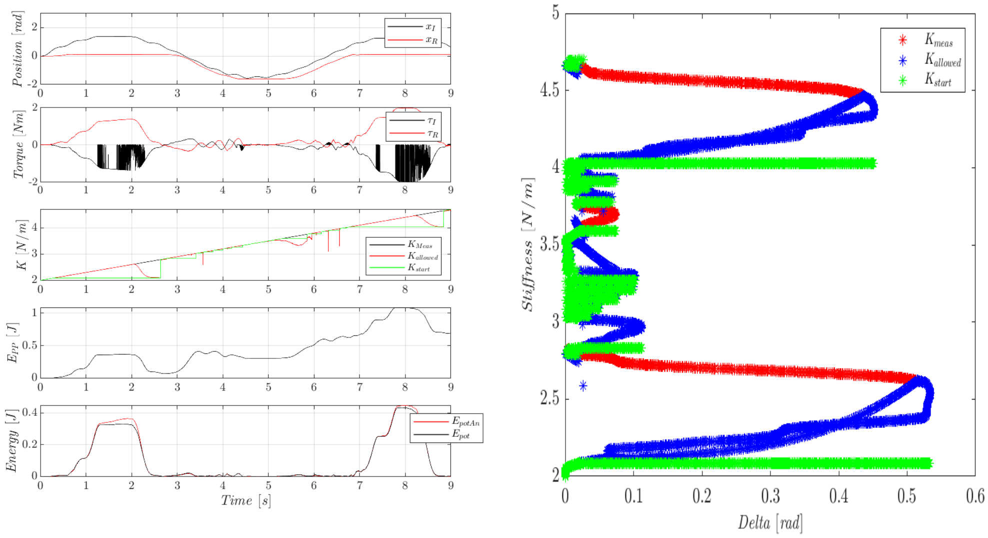

a) Constant increase in stiffness. **b)** Plot of Stiffness vs Deflection.

Figure 4.21: TDPA with nonlinear gradient subjected to variable stiffness under 200ms delay with wall contact.

figure 4.21a represents stiffness variation (Ramp input) in TDPA with Non-linear gradient. The position drift can be observed in this case at t=[5s,9s] because of the admittance type PC and higher time delay in the communication channel. The energy plot E_{PP} is always positive and thus confirms the passivity of the system despite the variable stiffness input. figure 4.21b shows the plot of Stiffness vs Deflection. It can be observed that at higher deflection during the pressing path the $K_{allowed}$ follows the K_{Meas} but during the releasing path it drops in a parabolic path and reaches to K_{start}. This avoids energy generation in the system due to variable stiffness and reduces the feedback force to the user.

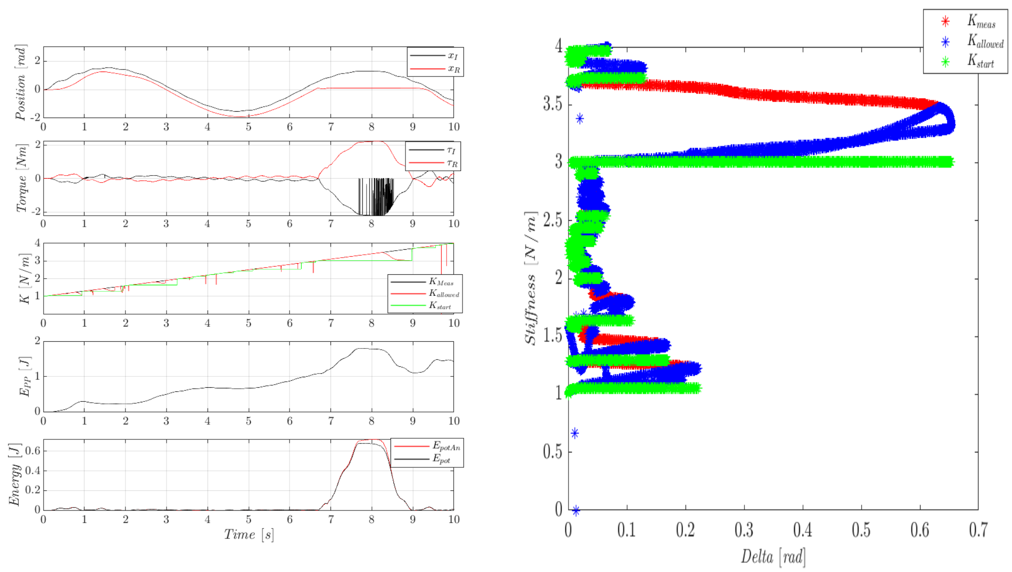

a) Constant increase in stiffness. **b)** Plot of Stiffness vs Deflection.

Figure 4.22: TDPA with nonlinear gradient subjected to variable stiffness under 200ms delay with free motion and wall contact.

figure 4.22a can be observed that the position synchronization is not perfect during free motion(t=[0s,5s]) and wall contact (t=[5s,10s]) due to the presence of delay in the communication channel. This behavior results, to some extent, from the admittance type PC that causes a position drift. High frequency force vibrations can be seen during the wall contact, which is caused by the impedance PC on the main device side, this tends to increase with time-delay. E_{PP} is always positive and thus confirms the passivity of the system. figure 4.22b indicates the plot of Stiffness vs Deflection, that shows the behavior of stiffness throughout the operation. At higher deflection,the allowable stiffness ($K_{allowed}$) adopts a non-linear path during releasing phase and reaching (K_{start}) can be observed. This prevents injection of energy in the system and hence maintain stability.

Discussion

The results presented in the previous section depicts the advantages of implementing Non-linear gradient concept with standard TDPA. The system remains passive for all the considered cases of stiffness variation and delays, but severe drift in the position can be observed in all the cases due to the presence of admittance type PC at the secondary device side. High frequency force vibrations can be seen during the wall contact, which is caused by the impedance PC on the main device side, this tends to increase with time-delay. This effect can be eliminated by using low pass filter or by adopting observer based gradient (OBG) method [13] .

Chapter 5

Experimental Validation

In this chapter the experimental setup used for testing and validation is described (see figure 5.1).

5.1 Experimental Setup

Teleoperation hardware

The system developed by SENSO-DRIVE GmBH mainly consists of two independent Motor units featuring torque sensors. Both devices are brushless with a nominal torque of 0.7Nm and a peak torque of 2 Nm. This system runs on real time operating system (QNX) at a frequency of 1KHz. A Simulink based user interface has been developed for rapid development and real time prototyping. The table below represents the main hardware features.

Table 5.1: 1 DOF Main and Secondary device characteristics

Bus Interface	CAN or ethercat
Operational frequency	1kHZ
Nomianal torque	0.7Nm
Pick torque	2Nm
Weight	500 gr
Dimensions	120 x 220 x 220 mm
Motor characteristics	Brushless DC

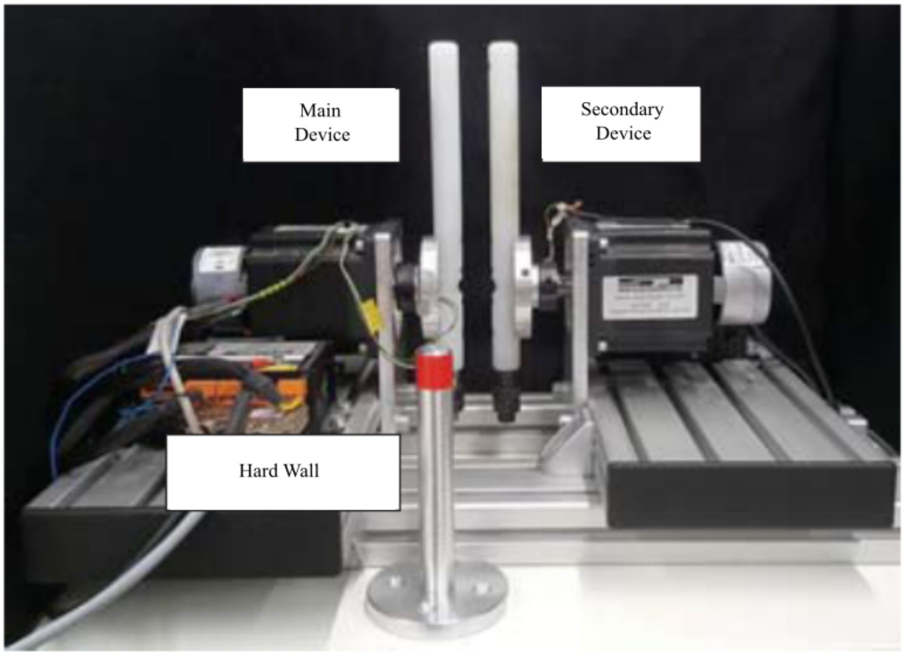

Figure 5.1: Experimental setup: Two 1-DoF rotational devices.

EMG Hardware

Figure 5.2: EMG hardware : Myo band device

The device features EMG electrodes, a 9-axes IMU composed of a 3-axes accelerometer, a 3-axes gyroscope, and a 3-axes magnetometer, and a vibration motor used to alert the user when a particular event occurs. The estimated stiffness from the EMG hardware (Myoband device) is sent to the one-DOF device via UDP communication and the experiments are performed accordingly. Similar to the machine learning algorithms used by the authors in [33] in our approach to stiffness estimation, we are using a ridge regression algorithm with a pseudo-Gaussian kernel that uses an approximation based on Random Fourier Features (RFF). As for the reasons, machine learning algorithm is used on the wrist rather than adopting co-contraction index based method in[12], this is because, in general, the forearm is, fairly hard to model, and agonistic and antagonistic muscles responsible for movements (and therefore stiffness) around a given axis are hard to identify. Therefore, machine learning approach is probably the most practical solution for stiffness estimation on the forearm. The limited mass of the hand and restricted range of motion of the wrist also contribute to making machine learning more effective. On shoulder and elbow, conversely, the muscle groups are probably easier to locate, and therefore for those joints a model-based approach can be more easily adopted. As the stiffness is measured in one dimension, there is no need to project the joint stiffness onto the cartesian space as described in [43], but a normalization and signal conditioning step in the form of a gain and offset in simulink model is introduced. This gain, which can be adjusted on the fly, in association with the linear regression model, amounts to essentially the same result. That is, one can adjust the gain so that the actual control impedance is sensibly controlled, independently of the actual estimated human stiffness in terms of its relation to the actual physical value.

5.2 Experiments

5.2.1 EMG stiffness estimation

In this section the stiffness estimated from the EMG hardware is used as an input to validate the concept of Non-linear gradient and the simulation results are plotted accordingly.

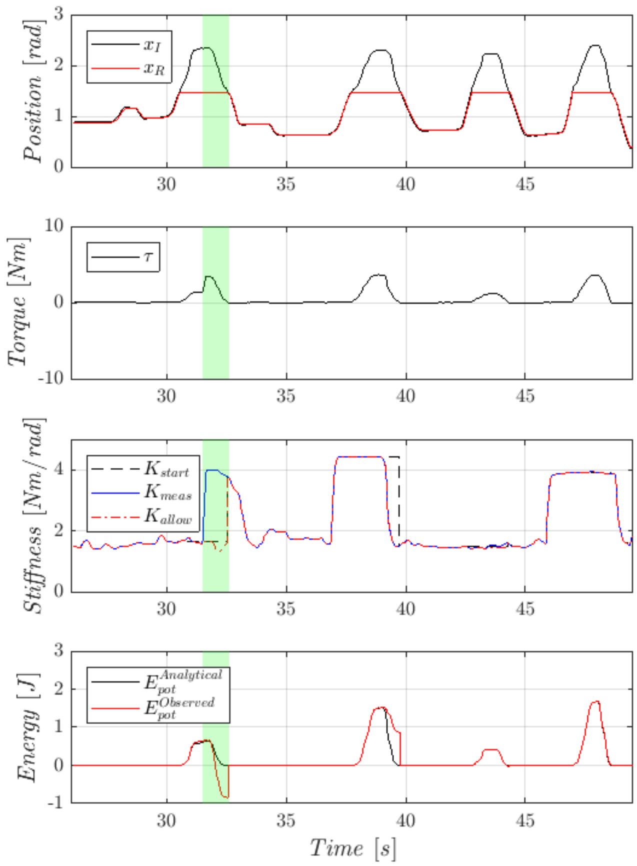

Figure 5.3: Passive variable impedance control with Passvity control OFF: Estimated stiffness from EMG hardware used as an input to Non-linear gradient control.

It can be seen in figure 5.3 that using the Non-linear gradient concept, the net energy output quickly decreases to negative values, if the passivity control (PC) is turned off and thus the system shows active behavior due to stiffness variation.

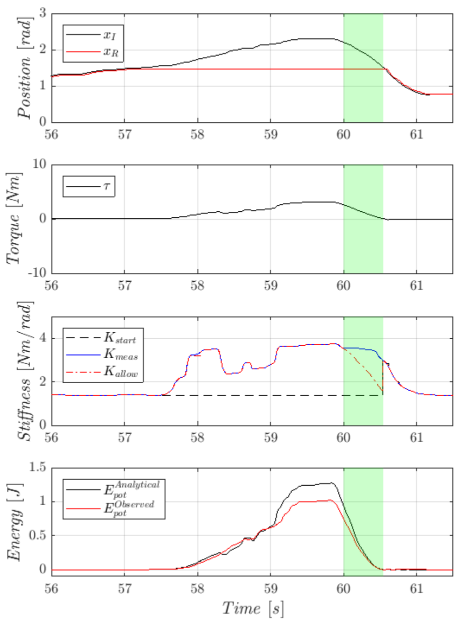

Figure 5.4: Soft in, stiff out with passivity control ON

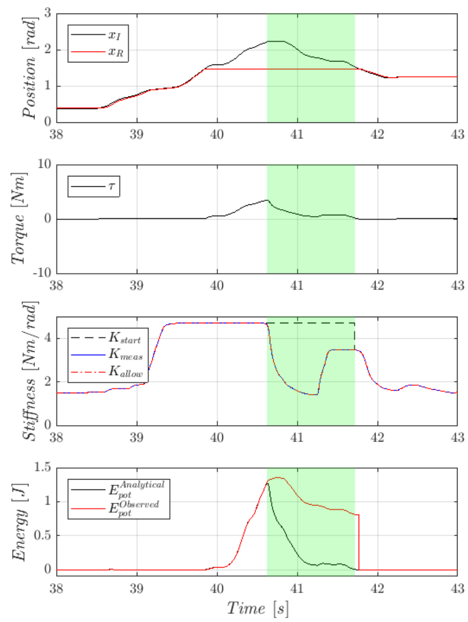

Figure 5.5: Stiff in, soft out with passivity control ON

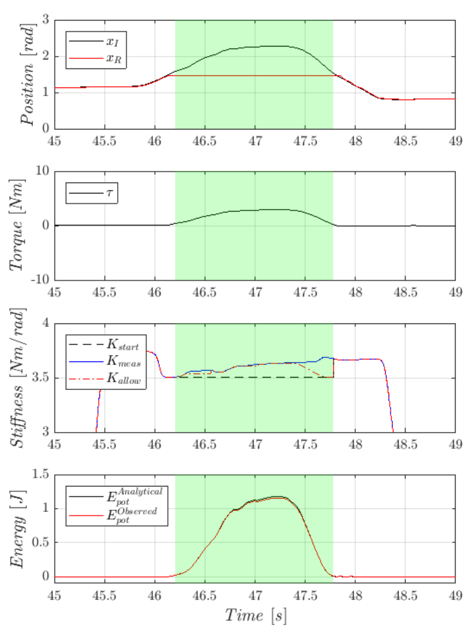

Figure 5.6: Constant stiffness with passivity control ON

In figure 5.4 the stiffness is increased during the releasing path compared to the pressing path (soft in,stiff out) the observed potential energy ($E_{pot}^{observed}$) is less than the analytical potential energy ($E_{pot}^{Analytical}$) and the K_{allow} drops based on the computed non-linear gradient during the releasing phase. The net energy output is positive and the system remains passive (with passivity control ON) throughout the whole operation even with stiffness variation.
In this figure 5.5 the stiffness is increased during the pressing phase than compared to the releasing phase (stiff in,soft out) and the observed potential energy ($E_{pot}^{observed}$) is higher than the analytical potential energy ($E_{pot}^{Analytical}$). The K_{allow} follows the K_{Des} and hence the desirable stiffness can be achieved during releasing phase. The net energy output is positive and the system remains passive (with passivity control ON) in this case.
In the case of constant stiffness input (see figure 5.6) the higher kinetic energy generation does not occur after contact and the observed potential energy ($E_{pot}^{observed}$) is approximately equal to analytical potential energy ($E_{pot}^{Analytical}$). A minimal K_{allow} drop during the releasing phase can be observed. The system remains passive (with passivity control ON) in this scenario.

5.2.2 Delayed Teleoperation

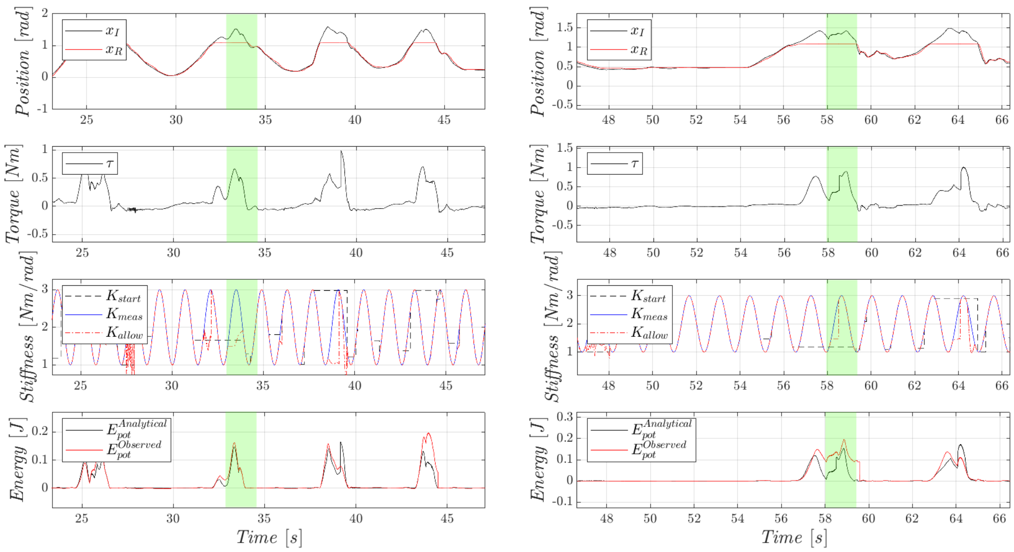

a) with time delay $T_d = 400$ms **b)** with time delay $T_d = 800$ms

Figure 5.7: The plots of a) and b) represents the sinusoidal stiffness variation in TDPA-ER with wall contact under different time delay.

The experimental results presents the wall contact scenarios at 400ms round-trip delay (see figure 5.7a) and 800ms round-trip delay (see figure 5.7b). The green area indicates the contact release intervals and it can be observed that analogous to TDPA-ER method the sudden dropping of main device force is absent during the releasing path due to the application of gradient methods. It can also be seen that the allowable stiffness ($K_{allowed}$) drops during the releasing path and resets back to its initial condition (K_{meas}) during free motion. The net observed potential energy($E_{pot}^{observed}$) is always positive and thus the passivity condition is satisfied.

5.3 Final remarks

In this chapter, the experimental results show the effectiveness of the proposed gradient method for both teleoperation with EMG hardware and delayed teleoperation scenarios.

In the first experiment, it can be observed that optimal results can be seen for different cases of stiffness variation that is estimated from the EMG hardware, which is attached to the user's arm. The observed potential energy ($E_{pot}^{observed}$) varies in response to the stiffness variation during pressing and releasing path, but in all the cases the net energy remains positive and thus ensures the passivity of the system.

In the second experiment, the gradient method is evaluated with higher time delays in combination with the least conservative approach TDPA-ER. The position synchronization is accurate even in the presence of higher time delays and sinusoidal stiffness variations. The drift in the position cannot be seen due to usage of impedance type PC on both the side of the devices. The sudden force drops as observed previously during the releasing path (see figure 4.5) are minimized with this combination of gradient method to TDPA-ER. The system remains passive for both the delayed cases (net observed E_{pot} is positive).

Chapter 6

Conclusion

In this thesis work, various control approaches are proposed to overcome the effects of variable stiffness in the bilateral teleoperation system. State-of-the-art TDPA method (TDPA-ER), Gradient methods are introduced, and the effectiveness of these methods are investigated more closely in simulation and experimental evaluations.

6.1 Summary

In the introduction, in order to perform a safer operation, the need for variable impedance or Tele-impedance was explained. However, variation of impedance according to the estimated stiffness from the human's arm in real-time leads to higher kinetic energy generation after contact with the environment and violates the passivity condition of the bilateral teleoperation system. To overcome these issues, the Time Domain Passivity Control methods are necessary. Within an extensive literature survey, similar systems, that involve stiffness estimation strategy and various control methods that are subjected to variable impedance are highlighted.
The proposed methods in this thesis, that is TDPA-ER is least conservative and more physically comprehensive, it provides optimal results in terms of position synchronization, higher transparency with no drift in position, despite the variation in stiffness and higher time delay in the communication channel. However, this approach has its limitations, since the feedback force drops drastically during the releasing path or free-motion if there is no potential energy available in the monitoring unit. Therefore, the concept of

stiffness gradient has been adopted in this work to compensate for the drawbacks of TDPA-ER and prevent the generation of energy due to variable stiffness.
The effectiveness of this approach can be observed in the simulation environment and experimental results. It can be seen that by combining this approach with standard methods, the force is maintained much longer during the releasing path in contrast to TDPA-ER and thus facilitating smoother operation.

6.2 Outlook

In future work, the concept of teleimpedance approach can be adapted to a passive time-delayed teleoperation system in combination with stiffness gradient methods for 6 DOF robotic devices. The parameters such as the end-point stiffness and the position reference can be estimated in real-time by EMG hardware and position markers respectively from the human's arm and are provided to the secondary device to achieve safe and compliant interaction with the environment. Furthermore, the concept of stiffness gradient methods can be applied to energy tanks and damping injection methodologies.

Appendices

Appendix A

Extension of Gradient Concept

Adaptation during pressing phase

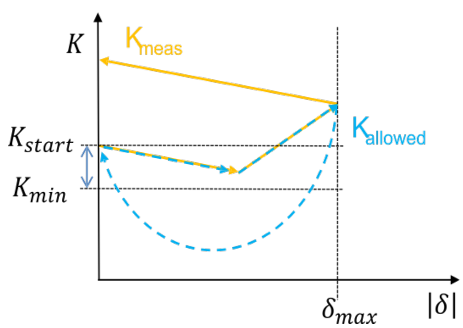

Figure A.1: Stiffness vs deflection plot

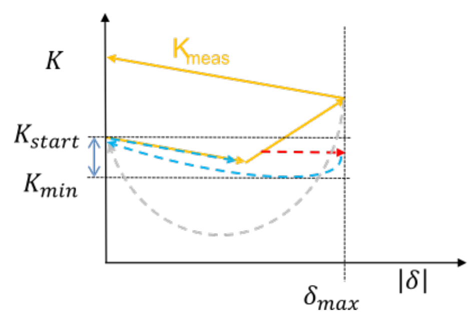

Figure A.2: Limitation of K_{allow} during pressing phase

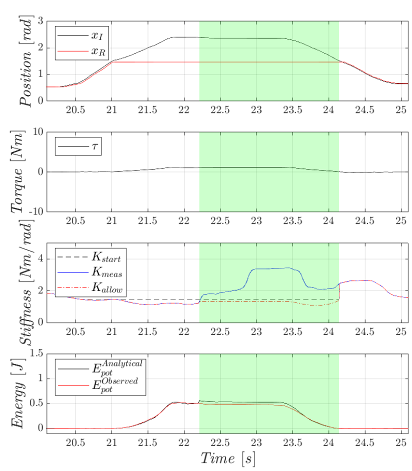

Figure A.3: Soft in, Stiff out with passivity controller ON

In certain cases of stiffness variation, it can be observed that during the releasing path the minimum point (K_{min}) of the computed allowable stiffness (K_{allow}) drops to a very lower value (see figure 1) and thus affecting the position synchronization between the devices and leads to sudden force jump in the system. In order to avoid this issue, the allowable stiffness can be limited during the pressing path as shown in figure 2 such that the K_{min} is limited during the releasing path and thus minimizing the force jump effects and improves the performance of the operation. The green area in the experimental result (see figure 3) represents the limitation of K_{allow} during the pressing phase to avoid the excess drop of allowable stiffness during the releasing phase.

Nomenclature

α Dissipation coefficient for an impedance based Passivity Controller

β Dissipation coefficient for an admittance based Passivity Controller

DOF Degrees of freedom

E_{L2R}^{M} Energy flowing into a TDPN from its left port (usually at the Main device)

E_{L2R}^{S} Energy flowing into a TDPN from its right port (usually at the Secondary device)

E_{R2L}^{M} Energy of a TDPN flowing out from its left port (usually at the Main device)

E_{R2L}^{S} Energy flowing into a TDPN from its right port (usually at the Secondary device)

F_e Environment force

F_m Main device force

F_s Secondary device force

$K_{allowed}$ Computed allowable stiffness during the releasing Phase

K_{Meas} Estimated or measured stiffness from the EMG hardware

K_{start} Stiffness during the start of the pressing Phase

P Power of the system

$P - Fc$ Position-Force computed architecture

$P - Fmeas$ Position-Force measured architecture

PC Passivity Controller

PO Passivity Observer

T_1 Forward time delay

T_2 Backward time delay

$TDPA$ Time Domain Passivity Approach

$TDPA - ER$ Time Domain Passivity Approach with Energy Reflection

v_m velocity of the Main Device

v_s velocity of the Secondary Device

Z_c Impedance of the controller

Z_e Impedance of the environment

Z_m Impedance of the Main Device

Z_s Impedance of the Secondary Device

CC Communication Channel

LTI Linear Time-Invariant

List of Figures

List of Tables

Bibliography

[1] D. Reintsema, K. Landzettel, and G. Hirzinger, "Dlr's advanced telerobotic concepts and experiments for on-orbit servicing," in *Advances in telerobotics*. Springer, 2007, pp. 323–345.

[2] P. Ridao, M. Carreras, E. Hernandez, and N. Palomeras, "Underwater telerobotics for collaborative research," in *Advances in telerobotics*. Springer, 2007, pp. 347–359.

[3] A. Bettini, P. Marayong, S. Lang, A. M. Okamura, and G. D. Hager, "Vision-assisted control for manipulation using virtual fixtures," *IEEE Transactions on Robotics*, vol. 20, no. 6, pp. 953–966, 2004.

[4] M. C. Çavuşoğlu, W. Williams, F. Tendick, and S. S. Sastry, "Robotics for telesurgery: Second generation berkeley/ucsf laparoscopic telesurgical workstation and looking towards the future applications," *Industrial Robot: An International Journal*, 2003.

[5] P. Marayong, M. Li, A. Okamura, and G. Hager, "D. kragic," *The International Journal of Robotics Research*, vol. 24, no. 9, pp. 731–741, 2005.

[6] B. Chebbi, D. Lazaroff, F. Bogsany, P. X. Liu, L. Ni, and M. Rossi, "Design and implementation of a collaborative virtual haptic surgical training system," in *IEEE International Conference Mechatronics and Automation, 2005*, vol. 1. IEEE, 2005, pp. 315–320.

[7] H. Esen, "Training in virtual environments via a hybrid dynamic trainer model," Ph.D. dissertation, Technische Universität München, 2007.

[8] B. Khademian and K. Hashtrudi-Zaad, "A four-channel multilateral shared control architecture for dual-user teleoperation systems," in *2007*

IEEE/RSJ International Conference on Intelligent Robots and Systems. IEEE, 2007, pp. 2660–2666.

[9] D. Morris, C. Sewell, F. Barbagli, K. Salisbury, N. H. Blevins, and S. Girod, "Visuohaptic simulation of bone surgery for training and evaluation," *IEEE Computer Graphics and Applications*, vol. 26, no. 6, pp. 48–57, 2006.

[10] L. Fabiani, G. Burdea, N. Langrana, and D. Gomez, "Human interface using the rutgers master ii force feedback interface," in *Proceedings of the IEEE 1996 Virtual Reality Annual International Symposium.* IEEE, 1996, pp. 54–59.

[11] A. Pillarisetti, M. Pekarev, A. D. Brooks, and J. P. Desai, "Evaluating the role of force feedback for biomanipulation tasks," in *2006 14th Symposium on Haptic Interfaces for Virtual Environment and Teleoperator Systems.* IEEE, 2006, pp. 11–18.

[12] A. Ajoudani, M. Gabiccini, N. Tsagarakis, A. Albu-Schäffer, and A. Bicchi, "Teleimpedance: Exploring the role of common-mode and configuration-dependant stiffness," in *2012 12th IEEE-RAS International Conference on Humanoid Robots (Humanoids 2012).* IEEE, 2012, pp. 363–369.

[13] H. Singh, A. Jafari, and J.-H. Ryu, "Enhancing the force transparency of time domain passivity approach: Observer-based gradient controller," in *2019 International Conference on Robotics and Automation (ICRA).* IEEE, 2019, pp. 1583–1589.

[14] T. Haidegger, B. Benyó, L. Kovács, and Z. Benyó, "Force sensing and force control for surgical robots," *IFAC Proceedings Volumes*, vol. 42, no. 12, pp. 401–406, 2009.

[15] D. A. Lawrence, "Stability and transparency in bilateral teleoperation," *IEEE transactions on robotics and automation*, vol. 9, no. 5, pp. 624–637, 1993.

[16] B. Hannaford and J.-H. Ryu, "Time-domain passivity control of haptic interfaces," *IEEE transactions on Robotics and Automation*, vol. 18, no. 1, pp. 1–10, 2002.

[17] J. Artigas, J.-H. Ryu, and C. Preusche, "Time domain passivity control for position-position teleoperation architectures," *Presence: Teleoperators and Virtual Environments*, vol. 19, no. 5, pp. 482–497, 2010.

[18] J. Artigas, R. Balachandran, C. Riecke, M. Stelzer, B. Weber, J.-H. Ryu, and A. Albu-Schaeffer, "Kontur-2: force-feedback teleoperation from the international space station," in *2016 IEEE International Conference on Robotics and Automation (ICRA)*. IEEE, 2016, pp. 1166–1173.

[19] J. Rebelo and A. Schiele, "Time domain passivity controller for 4-channel time-delay bilateral teleoperation," *IEEE transactions on haptics*, vol. 8, no. 1, pp. 79–89, 2014.

[20] J. Villanova i Buxó, "Time domain passivity-based telepresence with time delay," Ph.D. dissertation, Universitat Ramon Llull, 2005.

[21] E. Stoll, U. Walter, J. Artigas, C. Preusche, P. Kremer, G. Hirzinger, J. Letschnik, and H. Pongrac, "Ground verification of the feasibility of telepresent on-orbit servicing," *Journal of Field Robotics*, vol. 26, no. 3, pp. 287–307, 2009.

[22] B. Hannaford, J.-H. Ryu, D.-S. Kwon, Y. S. Kim, and J.-B. Song, "Testing time domain passivity control of haptic enabled systems," in *Experimental Robotics VIII*. Springer, 2003, pp. 550–559.

[23] J.-H. Ryu, D.-S. Kwon, and B. Hannaford, "Stability guaranteed control: Time domain passivity approach," *IEEE Transactions on Control Systems Technology*, vol. 12, no. 6, pp. 860–868, 2004.

[24] K. Hertkorn, T. Hulin, P. Kremer, C. Preusche, and G. Hirzinger, "Time domain passivity control for multi-degree of freedom haptic devices with time delay," in *2010 IEEE International Conference on Robotics and Automation*. IEEE, 2010, pp. 1313–1319.

[25] J.-H. Ryu, J. Artigas, and C. Preusche, "A passive bilateral control scheme for a teleoperator with time-varying communication delay," *Mechatronics*, vol. 20, no. 7, pp. 812–823, 2010.

[26] J. A. Esclusa, "Time domain passivity control for delayed teleoperation," Ph.D. dissertation, Ph. D. dissertation, PhD thesis, Universidad Politécnica de Madrid, 2014.

[27] J. Artigas, J.-H. Ryu, and C. Preusche, "Position drift compensation in time domain passivity based teleoperation," in *2010 IEEE/RSJ International Conference on Intelligent Robots and Systems*. IEEE, 2010, pp. 4250–4256.

[28] V. Chawda, H. Van Quang, M. K. O'Malley, and J.-H. Ryu, "Compensating position drift in time domain passivity approach based teleoperation," in *2014 IEEE Haptics Symposium (HAPTICS)*. IEEE, 2014, pp. 195–202.

[29] A. Coelho, H. Singh, T. Muskardin, R. Balachandran, and K. Kondak, "Smoother position-drift compensation for time domain passivity approach based teleoperation," in *2018 IEEE/RSJ International Conference on Intelligent Robots and Systems (IROS)*. IEEE, 2018, pp. 5525–5532.

[30] M. Panzirsch, J.-H. Ryu, and M. Ferre, "Reducing the conservatism of the time domain passivity approach through consideration of energy reflection in delayed coupled network systems," *Mechatronics*, vol. 58, pp. 58–69, 2019.

[31] J.-H. Ryu and C. Preusche, "Stable bilateral control of teleoperators under time-varying communication delay: Time domain passivity approach," in *Proceedings 2007 IEEE International Conference on Robotics and Automation*. IEEE, 2007, pp. 3508–3513.

[32] M. Panzirsch, J. Artigas, J.-H. Ryu, and M. Ferre, "Multilateral control for delayed teleoperation," in *2013 16th International Conference on Advanced Robotics (ICAR)*. IEEE, 2013, pp. 1–6.

[33] A. Gijsberts, R. Bohra, D. Sierra González, A. Werner, M. Nowak, B. Caputo, M. A. Roa, and C. Castellini, "Stable myoelectric control of a hand prosthesis using non-linear incremental learning," *Frontiers in neurorobotics*, vol. 8, p. 8, 2014.

[34] A. Gijsberts and G. Metta, "Incremental learning of robot dynamics using random features," in *2011 IEEE International Conference on Robotics and Automation*. IEEE, 2011, pp. 951–956.

[35] A. Rahimi and B. Recht, "Uniform approximation of functions with random bases," in *2008 46th Annual Allerton Conference on Communication, Control, and Computing*. IEEE, 2008, pp. 555–561.

[36] D. Sierra González and C. Castellini, "A realistic implementation of ultrasound imaging as a human-machine interface for upper-limb amputees," *Frontiers in neurorobotics*, vol. 7, p. 17, 2013.

[37] F. Ferraguti, C. Secchi, and C. Fantuzzi, "A tank-based approach to impedance control with variable stiffness," in *2013 IEEE international conference on robotics and automation*. IEEE, 2013, pp. 4948–4953.

[38] V. D. S. Stramigioli, "Port-based asymptotic curve tracking for mechanical systems."

[39] M. Franken, S. Stramigioli, S. Misra, C. Secchi, and A. Macchelli, "Bilateral telemanipulation with time delays: A two-layer approach combining passivity and transparency," *IEEE transactions on robotics*, vol. 27, no. 4, pp. 741–756, 2011.

[40] A. Franchi, C. Secchi, H. I. Son, H. H. Bulthoff, and P. R. Giordano, "Bilateral teleoperation of groups of mobile robots with time-varying topology," *IEEE Transactions on Robotics*, vol. 28, no. 5, pp. 1019–1033, 2012.

[41] Y. Michel, C. Ott, and D. Lee, "Passivity-based variable impedance control for redundant manipulators," in *in Proc. IFAC World Congress (IFAC)*, 2020.

[42] A. Dietrich, C. Ott, and S. Stramigioli, "Passivation of projection-based null space compliance control via energy tanks," *IEEE Robotics and automation letters*, vol. 1, no. 1, pp. 184–191, 2015.

[43] C. Castellini, A. Arquer, and J. Artigas, "semg-based estimation of human stiffness: Towards impedance-controlled rehabilitation," in *5th IEEE RAS/EMBS International Conference on Biomedical Robotics and Biomechatronics*. IEEE, 2014, pp. 604–609.

[44] X. Xu, C. Schuwerk, and E. Steinbach, "Passivity-based model updating for model-mediated teleoperation," in *2015 IEEE International Conference on Multimedia & Expo Workshops (ICMEW)*. IEEE, 2015, pp. 1–6.

[45] C. Pacchierotti, A. Tirmizi, G. Bianchini, and D. Prattichizzo, "Enhancing the performance of passive teleoperation systems via cutaneous feedback," *IEEE transactions on haptics*, vol. 8, no. 4, pp. 397–409, 2015.

[46] F. Ferraguti, N. Preda, A. Manurung, M. Bonfe, O. Lambercy, R. Gassert, R. Muradore, P. Fiorini, and C. Secchi, "An energy tank-based interactive control architecture for autonomous and teleoperated robotic surgery," *IEEE Transactions on Robotics*, vol. 31, no. 5, pp. 1073–1088, 2015.

[47] L. Meli, C. Pacchierotti, and D. Prattichizzo, "Experimental evaluation of magnified haptic feedback for robot-assisted needle insertion and palpation," *The International Journal of Medical Robotics and Computer Assisted Surgery*, vol. 13, no. 4, p. e1809, 2017.

[48] D. Lee and K. Huang, "Passive-set-position-modulation framework for interactive robotic systems," *IEEE Transactions on Robotics*, vol. 26, no. 2, pp. 354–369, 2010.